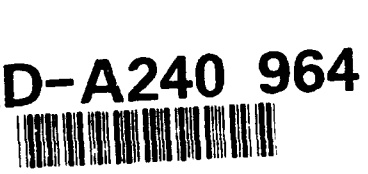

(2)

TECHNICAL REPORT RD-SS-91-7

FURTHER APPLICATIONS OF A CRYSTAL LATTICE DISINTEGRATION CRITERION TO PREDICT SHOCK-INDUCED REACTIVE CONDITIONS IN SOLID MATERIALS

James P. Billingsley
System Simulation and Development
Research, Development, and Engineering Center

July 1991

U.S. ARMY MISSILE COMMAND
Redstone Arsenal, Alabama 35898-5000

Approved for public release; distribution is unlimited.

DESTRUCTION NOTICE

FOR CLASSIFIED DOCUMENTS, FOLLOW THE PROCEDURES IN DoD 5200.22-M, INDUSTRIAL SECURITY MANUAL, SECTION II-19 OR DoD 5200.1-R, INFORMATION SECURITY PROGRAM REGULATION, CHAPTER IX. FOR UNCLASSIFIED, LIMITED DOCUMENTS, DESTROY BY ANY METHOD THAT WILL PREVENT DISCLOSURE OF CONTENTS OR RECONSTRUCTION OF THE DOCUMENT.

DISCLAIMER

THE FINDINGS IN THIS REPORT ARE NOT TO BE CONSTRUED AS AN OFFICIAL DEPARTMENT OF THE ARMY POSITION UNLESS SO DESIGNATED BY OTHER AUTHORIZED DOCUMENTS.

TRADE NAMES

USE OF TRADE NAMES OR MANUFACTURERS IN THIS REPORT DOES NOT CONSTITUTE AN OFFICIAL ENDORSEMENT OR APPROVAL OF THE USE OF SUCH COMMERCIAL HARDWARE OR SOFTWARE.

Unclassified

SECURITY CLASSIFICATION OF THIS PAGE

REPORT DOCUMENTATION PAGE

Form Approved OMB No. 0704-0188 Exp. Date: Jun 30, 1986

1a. REPORT SECURITY CLASSIFICATION: Unclassified	1b. RESTRICTIVE MARKINGS
2a. SECURITY CLASSIFICATION AUTHORITY	3. DISTRIBUTION/AVAILABILITY OF REPORT: Approved for public release; distribution is unlimited.
2b. DECLASSIFICATION/DOWNGRADING SCHEDULE	
4. PERFORMING ORGANIZATION REPORT NUMBER(S): TR-RD-SS-91-7	5. MONITORING ORGANIZATION REPORT NUMBER(S)
6a. NAME OF PERFORMING ORGANIZATION: Sys. Sim. & Dev. Dir., Res. Dev. & Engr. Center; 6b. OFFICE SYMBOL (If applicable): AMSMI-RD-SS	7a. NAME OF MONITORING ORGANIZATION
6c. ADDRESS (City, State, and ZIP Code): Commander, U.S.Army MICOM, Attn: AMSMI-RD-SS, Redstone Arsenal, AL 35898-5252	7b. ADDRESS (City, State, and ZIP Code)
8a. NAME OF FUNDING/SPONSORING ORGANIZATION; 8b. OFFICE SYMBOL (If applicable)	9 PROCUREMENT INSTRUMENT IDENTIFICATION NUMBER
8c. ADDRESS (City, State, and ZIP Code)	10. SOURCE OF FUNDING NUMBERS: PROGRAM ELEMENT NO. / PROJECT NO. / TASK NO. / WORK UNIT ACCESSION NO

11. TITLE (Include Security Classification): Further Applications of a Crystal Lattice Disintegration Criteria to Predict Shock Induced Reactive Conditions in Solid Materials

12. PERSONAL AUTHOR(S): James P. Billingsley

13a. TYPE OF REPORT	13b. TIME COVERED	14. DATE OF REPORT (Year, Month, Day)	15. PAGE COUNT
Final	FROM Jan. 89 TO Jan. 90	July 1991	49

16. SUPPLEMENTARY NOTATION

17. COSATI CODES			18. SUBJECT TERMS (Continue on reverse if necessary and identify by block number)
FIELD	GROUP	SUB-GROUP	lattice fracture, explosive, PBX-9407, PETN, shocked solids, detonation, octol, iron, crystal lattice, TNT, PPMI, NaCl

19. ABSTRACT (Continue on reverse if necessary and identify by block number)

As a follow-on to Reference 1, a threshold particle velocity, V_f, criteria derived by E.R. Fitzgerald [2] for the beginning of crystal Lattice Disintegration Phenomena (LDP) has been applied to additional shocked energetic and inert materials. The computed LDP shock pressures, Ps_f, compare rather well with experimental "threshold" shock pressures for four solid high explosives. The four explosives are: TNT, PBX-9407, octol, and PETN. The experimentally observed decrease of the detonation "threshold" shock pressure as the explosives decrease in density is predicted reasonably well for these explosives. Consequently, it is plausible that LDP is a significant factor in the initiation of detonation in shocked explosives. (continued next page)

20. DISTRIBUTION/AVAILABILITY OF ABSTRACT: ☒ UNCLASSIFIED/UNLIMITED ☐ SAME AS RPT. ☐ DTIC USERS	21. ABSTRACT SECURITY CLASSIFICATION: Unclassified
22a. NAME OF RESPONSIBLE INDIVIDUAL: Dr. James P. Billingsley	22b. TELEPHONE (Include Area Code): (205) 876-5210; 22c. OFFICE SYMBOL: AMSMI-RD-SS-AA

DD FORM 1473, 84 MAR — 83 APR edition may be used until exhausted. All other editions are obsolete.

SECURITY CLASSIFICATION OF THIS PAGE

Unclassified

19. Abstract (Continued)

In Reference 1, it was postulated that LDP was also responsible for phase changes, increased chemical reactivity, and anomalous electrical activity, which are experimentally observed in certain inert materials under relatively low–level shock–loading. This postulation is supported by the present LDP assessment results for shocked PPMI, iron, and NaCl. As such, Fitzgerald's LDP V_f is strongly believed to be the "trigger mechanism" responsible for the low pressure "catastrophic shock" and consequent "bond scission" event suggested by Graham [26], which was based on many experimental observations.

The importance of the De Broglie momentum–wave length relation with respect to particle velocity propagation in shock–loaded solid materials is emphasized via the results reported in this document.

Acknowledgements

It is a pleasure to express appreciation to the following individuals who supplied vital technical reports, papers, and unpublished test information necessary to complete this investigation.

- Dr. Richard J. Wasley, Lawrence Livermore National Laboratory; [15]

- Dr. J. J. Dick, Los Alamos National Laboratory; [23, prior to publication in a conference proceeding].

- Dr. Steve Sheffield, Los Alamos National Laboratory; ([19, 28], which is experimental shock and particle velocity data for PPMI, shown in Figure 6)

- Dr. M. Van Thiel, Lawrence Livermore National Laboratory; [42]

- Dr. E. R. Fitzgerald, Johns Hopkins University, ([3; 4; 55; 60; 61; 62], and encouragement to continue this research).

- Mr. H. C. Rodean, Lawrence Livermore National Laboratory, for reviewing a draft of Appendix B and supplying a copy of a technical journal article.

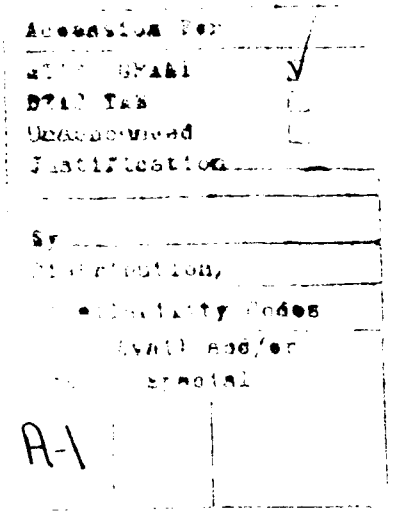

TABLE OF CONTENTS

LIST OF ILLUSTRATIONS

LIST OF TABLES

1. INTRODUCTION

Reference 1 documents the application and extension of Fitzgerald's crystal lattice disintegration criteria [2, 3, 4] to shock–loaded solid reactive and inert materials. In Reference 1, six explosives (comp–B3, comp–B, pressed TNT, tetryl, H–6, and PBX–9404) and one inert material (PMMA or plexiglas II) were investigated. It was tentatively concluded that crystal lattice disintegration was responsible for the experimentally observed response which occurred at certain shock pressure (Ps) levels.

To further investigate this initial conclusion, additional available experimental data for several reactive (explosive) and inert materials have been examined, and the important particle velocities (V_1 and V_f) were computed. The associated shock velocity (Us_f) and shock pressure (Ps_f) were also calculated to facilitate comparison with experimentally observed reactive or anomalous events.

The explosives analyzed are: pressed TNT, PBX–9407, octol, pressed PETN, and crystal PETN. Pressed TNT was considered again because some important experimental information was found since the publication of Reference 1.

Three rather diverse inert materials are considered. They are: poly pyromellitimide (PPMI), iron, and sodium chloride (NaCl). PPMI is a complex polymeric compound whose low–pressure shock–loading behavior is highly non–linear. Iron and NaCl have both been extensively investigated via shock–loading experimentation. The results have been controversial, unexpected, and usually inexplicable, since both of these rather common substances exhibit exceptionally complex behavior under shocked conditions.

The present suggestion that Lattice Disintegration Phenomena (LDP) or atomic bond breaking V_f effects are a "root cause" for low pressure shock induced reactions may also be controversial. However, the number of favorable comparisons of predicted and experimental information, contained in this report and in Reference 1, is more than could reasonably be expected from mere chance or fortuitous circumstances. Four of the nine different explosives have been analyzed for two different densities, which makes a total of 13 comparative cases for the energetic materials. There are 17 examples in all when the four inert materials are included.

2. METHODOLOGY

Essentially, in Reference 1, the microscopic particle velocities analyzed in Reference 2 (Chapter 3) were considered equivalent to the macroscopic particle velocities, Up, observed experimentally in shocked solid materials [5]. Consequently, the critical particle velocity, V_f, for lattice break–up and disintegration, derived in Chapter 3 of Reference 2, could be related to a corresponding shock wave velocity, Us_f, and shock pressure, Ps_f, by the following equations:

$$Us_f = Co + S * V_f \tag{1}$$

$$Ps_f = \rho_o \, Us_f \, V_f \tag{2}$$

Equation 1 simply states the experimentally observed fact that the shock wave velocity, Us_f, is a linear function of the particle velocity, Up, for many shock–loaded materials [5, Eq. 7]. Co and S are both constants and have been experimentally determined for a large number of materials [5].

The shock velocity may be a nonlinear function of the particle velocity for certain substances. In that case, Us can be found from tables or graphs of Us as a function of Up. Table 1 contains Co and S information for the shocked explosives and materials considered in this report. The sources of this information are also listed.

Equation 2 is the well known expression for shock pressure [5, Eq. 2]. Ps_f is the product of the material density (ρ_o), shock velocity (Us_f), and the particle velocity (V_f).

When V_1 is known, Us_f and Ps_f may be computed and compared with experimental data (Up, Us, Ps) corresponding to any phenomena which could be attributed to lattice disintegration or bond breakage. This is basically the approach followed in Reference 1 and in the present report.

The following relation for V_f was deduced by Fitzgerald [2, Chapter 3] from somewhat unusual particle dynamics concepts. He called this the phonon fission velocity, which is:

$$V_f = \frac{V_1 + \sqrt{V_1^2 + 4 * V_1 * C_s}}{2} \tag{3}$$

It is approximately equal to the geometric mean of V_1 and C_s since V_1 is normally much less than C_s so that:

$$V_f \approx \sqrt{V_1 * C_s} \tag{4}$$

The velocities V_1 and C_s are defined as follows:

$$V_1 = \frac{h}{2 \, m \, d_1} \tag{5}$$

V_1 = The De Broglie particle velocity which is the limiting free particle velocity which can occur without permanent lattice deformation (plastic flow); or the limit propagation velocity for particle–momentum waves in a stationary lattice. See References 6 and 68 for additional information.

$$C_s = \sqrt{\frac{2 * C_t^2 + C_L^2}{6}} \qquad (6)$$

= A mean sound velocity defined such that the cohesive energy, D, per atom of mass, m, is $m C_s^2$. See Appendix B for additional information.

The quantities appearing on the right–hand side of Equations 5 and 6 are defined as follows:

h = Planck's constant

$$= 6.6262 \times 10^{-27} \frac{(\text{gram})\ (\text{cm}^2)}{\text{sec}}$$

d_1 = Closest distance between the atoms in a crystal lattice, or the atomic spacing in a slip direction. Units are angstrom units, Å (Å = 10^{-8} cm).

m = Mass of one atom, grams.

C_t = Elastic transverse or shear wave velocity, cm/μ – sec.

C_L = Elastic longitudinal wave velocity, cm/μ – sec.

A more general expression for C_s is given in Reference 3 for materials which do not exhibit uniform accoustical wave propagation characteristics in three orthogonal directions. This relation, from Equation 9 of Reference 3 is:

$$C_s = \sqrt{\frac{C_{L1}^2 + C_{t1a}^2 + C_{t2b}^2 + C_{L2}^2 + C_{t2a}^2 + C_{t2b}^2 + C_{L3}^2 + C_{t3a}^2 + C_{t3b}^2}{18}} \qquad (7)$$

Note that Equation 7 reduces to Equation 6 if the three orthogonal longitudinal wave velocities (C_{L1}, C_{L2}, and C_{L3}) are equal, and the six shear wave velocities (C_{t1a}, C_{t1b}, C_{t2a}, C_{t2b}, C_{t3a}, C_{t3b}) are equal.

It is maintained in Reference 3 that if $m C_s^2$ is the bond energy per atom, D, then C_s^2 (or the sum of the squares of the six shear wave velocities and the three longitudinal wave velocities) must be an invariant quantity. The analysis in Reference 3 did not prove that $D = mC_s^2$, but it did show that C_s^2 was an invariant, which is a necessary condition for this relation to be valid.

A more general form of V_f was derived in Reference 2, Equation 3.17, which is:

$$V_f = \frac{V_1 + \sqrt{V_1^2 + 4 * V_1 * V_{Lf}}}{2} \qquad (8)$$

where

V_{Lf} = A velocity defined such that the lattice bond dissociation energy per atom of mass, m, is $k^* m^* V_{Lf}^2$, where k is a constant.

That is, in certain cases, V_{Lf} may not be equal to C_s as defined by Equations 6 and 7. One likely candidate for V_{Lf} could be C_b, the bulk elastic wave velocity. See Reference 47 and Appendix B.

It was empirically shown in Reference 2 for 18 metals, that the dissociation energy per atom, D, was equal to $m C_s^2$. This same idea (that $D = m C_s^2$) was considered (without proof) to be applicable to polymeric materials in the analysis reported in Reference 1 and in the present study also. The favorable comparisons of the computed and experimental reactive conditions documented in Reference 1 and the present report are consistent with this assumption. The credibility of this assumption is also enhanced via information found in Reference 69. Reference 69 contains estimates of the energy per gram ($E's = D/m$) required for complete vaporization of Comp–B and PBX–9404. For both explosives, $\sqrt{E's}$ compared reasonably well with C_s (Table B–2).

Fitzgerald's derivation of V_f is based on the premise that the De Broglie relation ($Up = h/(2m\, d'_1)$) must be satisfied for particle velocities greater than V_1. This led him to the unusual concepts of reverse lattice motion and the extraction/depletion of cohesive energy to create this motion. Consequently, this means that the De Broglie relation must be satisfied on a microscopic scale within the shock front thickness (a few angstroms) by either reverse lattice motion or some other phenomenon even more bizarre!

This is because the one–dimensional bulk shock compression [59, pp. 463–465] is definitely not sufficient to satisfy the De Broglie relation demands on the lattice spacing ($d'_1 = h/(2m\, U_p)$). The bulk unidimensional shock compression is:

$$\frac{d}{d_1} = \frac{\nu}{\nu_o} = \frac{\rho_o}{\rho} = \frac{Us - Up}{Us} \qquad (9)$$

so that:

$$d_1' << d \quad \text{when} \quad U_p > V_1 \qquad (10)$$

That is, the bulk shock compression from d_1 to d is much less than from d_1 to d_1'. In fact, the bulk shock compression (d_1 to d) is practically insignificant compared to the large change from d_1 to d_1'.

Perhaps the basic reason a shock wave (or shock front thickness) is formed is because De Broglie's relation must be satisfied for particle velocities greater than V_1. The shock front thickness does indeed seem to be very dense (or more dense than material fore and aft of the wave front). This is observed from photographs of shocks in transparent materials. Consequently, it is plausible to suggest that it is in the shock front thickness where the De Broglie velocity – wave length relation is satisfied (possibly during times on the order of 10^{-12} or 10^{-13} second). Subsequently, there would be material relaxation from d_1' to d (bulk compression) and eventually to d_1 as relaxation continues.

The remarks in the previous paragraph are believed to apply not only to solids, but to liquids and gases as well. Recent Computational Molecular Dynamics (CMD) numerical modeling results for shock loaded particles (atoms and/or molecules) are reported in References 63 through 67. It is recommended that numerical experimentation with Fitzgerald's LPD V_f concept be included in future CMD studies. The LPD cohesive energy dissipation is visualized as a damping influence which could possibly explain viscous effects within the shock front thickness [70] and the shock variable (Ps, Us, Up) decay observed as a function of distance traveled.

The important relationship of V_1 (the De Broglie particle velocity in an undisturbed or immobile lattice) with respect to the Hugoniot Elastic Limit (HEL) particle velocity (Up_{HEL}) observed in Elastic–Plastic Shock (EPS) experiments is discussed in Reference 6. It is shown in Reference 68 that critical particle velocities causing lead azide detonation are comparable to V_1, based on the nitrogen atom mass and nitrogen bond lengths for this compound.

This illustrates that refinements with respect to the computation of V_1 are feasible. Particular atoms or combinations of atoms and their associated minimum slip distances, d_1, may warrant special attention. For example, Fitzgerald in Reference 2, Chapter 3, computes a separate V_1 for each of the two atoms (Na and Cl) in salt (NaCl). Information necessary to make a judicious choice of the atom or atomic group in polymeric solids is required because of the large number of possible selections which may not be physically realistic. Theoretical and experimental attempts to delineate the atoms or atomic combinations which initialize reactions in explosive detonation phenomena are documented respectively in References 7 and 8. Other References reporting similar explorations could be cited.

The importance of specific atomic elements in shocked solids is very plausible in view of their very sensitive influence in vibrating bone structure [Appendix C].

When the particle velocity, Up, equals or exceeds V_f, self–sustained particle impact or fission is possible [2]. Fragments of the broken lattice will strike other lattice particles, and the process is repeated. Individual atoms could also be freed from their bonds and in turn strike other atoms or lattice fragments. Such an atom is called a "free atom" by Fitzgerald [4]. The travel of a "free atom" in the atomic lattice should satisfy the De Broglie demands even though the bulk particles of shocked materials may not do so. See above discussions of Equations 9 and 10 implications.

These "free atoms" in a shocked solid are not generated in a homogeneous array, but in a random heterogeneous manner. In a reactive or explosive material, these "free atoms" form localized "hot spots." When the concentration or number of hot spots (local particle impacts) per unit area reaches a critical value (dependent on the explosive), then the process is irreversible and detonation is inevitable.

Thus the LDP can be the threshold trigger mechanism that creates heterogeneous hot spots which in turn causes detonation in secondary explosives and observable reactions in many inert materials.

3. APPLICATIONS

In order to perform an assessment analysis for LDP effects, the following information is required. These data must be for the same material (i.e., same composition, same density, ρ_o, same manufacturing history, etc.).

	Item	Purpose
1.	m and d_1 or m_{AV} and d_{1AV}	To compute V_1 via Eq. 5
2.	C_L and C_t	To compute C_s, via Eq. 6 or 7 and V_f via Eq. 3
3.	$Us = f(U_p)$	To compute Us_f and Ps_f from V_f
4.	Experimental shock–induced reactive information as a function of Up, Us, and Ps	To compare with the predicted reactive conditions, V_f, Us_f, Ps_f, and V_1

Even though a voluminous amount of shock–loaded material information is available, it is difficult to assemble the above information for the same consistent material. However, enough sufficiently consistent information has been found for four energetic and three inert materials so that an LDP criteria analysis could be made. Table 1 lists Us = f (Up) information for all the materials investigated. If Us = f (Up) was not linear, then the data (Us vs. Up) was plotted and Us_f was graphically determined. See Appendix A for m_{AV} and d_{1AV} results.

Table 2 contains m, d_1, C_L, C_t, V_1, V_f, Us_f, and Ps_f information for the materials under consideration. Table 3 contains C_L, C_t information for one material, single crystal PETN.

Table 4 lists the comparable computed predicted and experimental observed reactive conditions for all the materials under investigation. Tables 1 through 4 also provide the sources of information for the tabulated data.

Figures 1 through 10 depict the results of this investigation and also indicate information sources. Reference 9 is a very valuable general information source for explosives. References 10 and 11 are well known sources for the Large Scale Gap Test (LSGT) and Small Scale Gap Test (SSGT) results, respectively, for explosive sensitivity.

Pertinent LDP V_f results for the energetic and inert materials are discussed in the following sections.

A. Energetic Materials

1. Pressed TNT

Pressed TNT (ρ_o = 1.635 g/cc) was considered in Reference 1. Since then, references 13, 14, and 15 were discovered, which contained consistent information for pressed TNT where ρ_o = 1.648 g/cc. Ps_f (20.5 kbars) compares very well with the experimental reaction results (P_R = 24 kbars) from Reference 15. Both of these data points are plotted in Figure 1 which also contains experimental data from References 10, 11, and 12. See Reference 1 which also discusses a similar figure (Fig. 3). References 12 and 15 utilized flat plate impact to shock

the TNT targets, and this provided precisely defined load conditions. The Ps_f values [1, present study] compare very favorably with the experimental results of References 12 and 15. This reinforces the conclusion, stated in Reference 1, that the LDP criteria provides an explanation for the observed increase of the detonation "threshold" shock pressure as the explosive density increases or porosity decreases.

2. PBX – 9407

Information contained in References 9 and 16 was sufficient for a consistent computation of V_f, Us_f, and Ps_f for PBX–9407 (ρ_o = 1.608 g/cc). From information in Reference 9, a consistent computation of V_f was made for ρ_o = 1.78 g/cc. However, the Us = f(Up) relationship was unknown for this density. Consequently, to make an approximate computation of Us_f and Ps_f for ρ_o = 1.78 g/cc, the U_s = f(Up) relation for ρ_o = 1.608 g/cc was employed. Consequently, it is believed that these approximate values of Us and Ps_f for ρ_o = 1.78 g/cc are somewhat smaller than they should be.

These Ps_f results are shown plotted as a function of density (ρ_o) in Figure 2. Also shown in Figure 2 are the SSGT results from Reference 11 and Lindstrom's asymptotic P_{MIN} result from Reference 16.

The Ps_f magnitudes are somewhat smaller than the SSGT P_D values, but the variation with density is very similar. The vertical arrow above the Ps_f point for ρ_o = 1.78 g/cc indicates that this magnitude should probably be somewhat greater than shown.

For ρ_o = 1.608 g/cc, Ps_f (11.1 kbars) and the P_{MIN} result from Reference 16 compare very well. P_{MIN} (9.35 kbars) is the average value of P_{MIN} from the time to detonation and distance to detonation curve fits. P_{MIN} is the minimum shock pressure necessary to cause detonation. This interpretation of P_{MIN} agrees with Lindstrom's alternate assumption with respect to P_{MIN} which is "that the pressure must be greater than some finite limit for detonation to occur."

3. Octol

Information contained in Reference 9 was sufficient to allow a consistent computation of V_f, Us_f, and Ps_f for cast octol (ρ_o = 1.80 g/cc). This value of Ps_f (24.74 kbars) is shown plotted in Figure 3 where it compares favorably to LSGT results for cast octol [10] and SSGT results for pressed octol [11].

4. PETN

An LDP assessment was made for both pressed and single–crystal (S. C.) pentaerythritol tetranitrate explosive which is commonly referred to as PETN. The assessment procedure for the pressed PETN is the same as for the PBX–9407, octol, and pressed TNT. However, for the S. C. PETN, a modification was incorporated in the computations. The illustration of this modification was one reason for including S. C. PETN in this report. Another reason is to show that LDP offers an explanation for certain rather low–level ($Ps \leq 40$ kbars) shock–induced reactions which have been experimentally observed in S. C. PETN.

a. Pressed PETN

Information contained in References 9 and 17 was sufficient for a consistent computation of V_1, V_f, Us_f, and Ps_f for pressed PETN (ρ_o = 1.72 g/cc), as shown in Tables 1 and 2. In Figure 4, Ps_f is graphically compared with test results from References 11 and 17. Ps_f

is somewhat larger than the SSGT results [11]. Ps_f (21.0 kbars) is still larger than the experimental detonation pressure (17.0 kbars) from Reference 17. This is considered a reasonably good comparison. It should be noted that although detonation was not observed [17] for Ps below 17.0 kbars, perhaps it would have been for larger sample sizes.

b. Single–Crystal PETN

Shock–loading experimentation with S. C. PETN has been documented in References 18 through 23. References 18, 20, and 21 mention that "anomalous" inexplicable reactions were observed in S. C. shocked with 40 kbars in the <110> direction. In fact, Reference 18 indicates that shock–induced decomposition may have occurred in two shots where the shock pressure was nominally 26 kbars. Certain characteristics of the transducer gauges (x–cut quartz) at these load levels prevented a definite resolution of the observed anomalies. A strong reaction at 40 kbars was also apparently observed by Craig [18, 20, 21].

The above reactions at 26 and 40 kbars were termed "anomalous" because they were inexplicable by conventional reaction rate theory. Apparently it normally required about 86 kbars to reliably detonate <110> S. C. PETN [18 through 22].

In order to clarify this situation, which had existed for a number of years, experimentation on S. C. PETN with 22.0, 35.0, and 42.6 kbars of shock input was performed [23] with the following results:

> 42.6 kbars: Detonation occurred. The sample crystal was larger than those employed by previous investigations. Two different shots were fired and the quartz gauge pressure records were practically identical to one recorded by Craig at 40.0 kbars [23, Fig. 1]. Consequently, it is assumed that detonation would have been observed at 40.0 kbars if the sample had been larger.
>
> 35.0 kbars: Strong light emission was observed. According to Reference 23, this is:
>
> "Strong evidence that we are observing nonequilibrium chemiluminescence due to shock–induced decomposition during the initiation process."
>
> 22.0 kbars: Light emission was observed, both for <110> and <001> orientations. This is indicative of some reaction at this level of shock–loading.
>
> These reactive pressure data points (22.0, 35.0, and 40.0 kbars) are shown in Figure 4 on the crystal Theoretical Maximum Density (TMD) indicator line. Also shown on the TMD line is the LDP Ps_f value (25.0 kbars) computed via the information contained in Tables 1, 2, and 3. The (Ps_f, V_f) point is plotted in Figure 5 along with the experimental results from Reference 18.

Note that because S. C. PETN is anisotropic, the value of C_s was computed via Equation 7 as shown in Table 3. The elastic wave velocities given by Morris [24] were employed in this computation. Note also that the average or "bulk" values of m and d_1 were

used to compute V_1. The "bulk V_1" LDP Ps_f prediction (25.0 kbars) is remarkably close to the experimentally observed light emission reaction pressure, P_R, level of 22.0 kbars.

It was stated in Section II and in Reference 1 that the contribution of individual atoms or atomic groups could be given special attention via the V_1 computation. Bond length distances between atoms in the PETN crystal are given in Reference 25. However, at present, the author does not possess sufficient information for a judicious choice of the correct atom or atomic combination to compute a more specific or appropriate V_1 than the "bulk V_1" based on average values. The required information is being sought, and when found, a more appropriate V_1 and the associated V_f, Us_f, and Ps_f values will be computed.

B. Inert Materials

1. PPMI

Information for a shock–loaded polymeric substance, PPMI, was acquired from References 26, 27, and 28. Sufficient consistent data were available so that an LDP assessment could be performed. In the particle velocity, Up, region of interest, the shock velocity, Us, is a non–linear function of Up as shown in Figure 6. From this figure, Us_f was determined when V_f was computed. Ps_f was 15.0 kbars which is very close to the "cusp" location [27, 28] of the Us = f(Up) relationship that occurs at about 18.0 kbars.

Reference 27 indicates that shock–induced polarization also begins at approximately 18.0 kbars for PPMI. Thus, both the Hugoniot cusp and the initial shock–induced polarization point is very close to the predicted LDP Ps_f point.

The authors of Reference 27 also refer to a shock Hugoniot cusp and shock–induced polarization in polymethyl methacrylate (PPMA), or plexiglas, which occurs at about 20.0 kbars. This coincides rather closely with the LDP Ps_f, predicted in Reference 1 for PPMA, which was 21.4 kbars.

In Reference 26, Graham presents a strong case for a "catastrophic shock" event which occurs at a relatively low shock pressure threshold. Above this pressure threshold, lattice or chemical "bond scission" and anomalous electrical phenomena occur in shocked polymeric solids. Furthermore, non–equilibrium thermodynamic conditions and process irreversibility exist during and after the "catastrophic shock" event.

Graham postulated that a "catastrophic shock" event was occurring, based upon his observations of a large amount of experimental data. However, a "trigger mechanism" for low–pressure "catastrophic shock" bond scissions has been difficult to justify theoretically via conventional shock physics theory.

Consequently, unconventional concepts such as Fitzgerald's LDP V_f criteria merit attention. In view of the "predictive power" demonstrated in Reference 1 and the present report for a number of diverse materials, it is believed that Fitzgerald's LDP V_f provides the "trigger mechanism" for the low–pressure "bond scissions" of the "catastrophic shock" event.

2. Iron

Reference 29 provides a comprehensive review of the technical literature up to 1977 with respect to shock–induced lattice–structure phase changes observed in solid materials.

The element, iron, was the first material in which a shock–induced phase change was found, and much experimental work has since been performed to delineate the phenomena which occurs at approximately 130.0 kbars.

Figures 7 and 8 illustrate experimental results for Us and Ps, respectively, as a function of particle velocity, Up, for shock–loaded iron. Sources [30 through 34], for the experimental information are denoted in these figures.

Iron, under moderate shock–loading below 130 kbars, exhibits a two–wave structure where the first one is essentially an elastic wave followed by a slower plastic deformation wave front. In general, this is called elastic–plastic shock phenomena (EPSP).

The elastic wave generated under EPSP conditions is called the HEL to distinguish it from a dynamic elastic limit which could occur from less severe transient load conditions [35]. It is noted in Reference 36, page 191, that the HEL condition can produce the same effect as a phase transition. That is, an additional wave is formed [6].

In order to perform an LDP assessment for iron, the velocities V_1 and V_f given in Table 3 were employed to compute Us_f and Ps_f. The double wave structure requires that these computations be performed via the following equations [35, p. 256].

The pressure behind the HEL wave is:

$$P_{HEL} = \rho_o C_L U_{PHEL} \tag{11}$$

$$= \rho_o C_L V_1 \tag{12}$$

It was shown in Reference 6 that the steady state equilibrium value of the HEL wave particle velocity, Up_{HEL}, was equal to V_1. The density behind the HEL wave is:

$$\varrho_{HEL} = \varrho_o \left(\frac{C_L}{C_L - Up_{HEL}} \right) \tag{13}$$

$$= \varrho_o \left(\frac{C_L}{C_L - V_1} \right) \tag{14}$$

$$\approx \varrho_o \tag{15}$$

Equation 15 is a good approximation because C_L, the longitudinal elastic wave velocity, is much larger than V_1 so that $C_L/(C_L - V_1) \approx 1.0$.

The plastic wave pressure corresponding to the LDP particle velocity, V_f, is:

$$Ps_f = \rho_{HEL} Us_f (V_f - U_{PHEL}) + P_{HEL} \tag{16}$$

$$Ps_f = \rho_{HEL}\, Us_f\, (V_f - V_1) + P_{HEL} \qquad (17)$$

The iron plastic wave velocity is a linear function of the particle velocity as given by Equation 1. The values of C_o and S, as recommended by References 33 and 34 are C_o = 4.63 km/sec and S = 1.33. This equation is plotted in Figure 7. For V_f = 0.22 km/sec, Us_f = 4.92 km/sec, and this point is shown in Figure 7. Also shown in Figure 7 is the HEL point defined by C_L and Up_{HEL}. Note that these values of C_L (6.04 km/sec) and Up_{HEL} (0.0140 km/sec, or essentially V_1, which is 0.0144 km/sec) are the same ones that Minshall [35] obtained experimentally for the thick iron specimen [6, Fig. 2]. The corresponding P_{HEL} via Equation 12 is 6.8 kbars.

For ρ_o = 7.84 g/cc, then ρ_{HEL} = 7.86 g/cc via Equation 14. All the information required to compute Ps_f via Equation 17 is now available. This computation yields Ps_f = 86.3 kbars. The (Ps_f, V_f) point is shown in Figure 8.

The predicted LDP initiation Ps_f location is also shown in Figure 9, which depicts experimental data for the relative electrical resistance (R/R_o) of shock–loaded iron as a function of the shock pressure, Ps. These experimental data are from References 37 and 38. The earlier results (1962) from Reference 38 show a rather abrupt jump in electrical resistance at 150 kbars, which is somewhat beyond the 130 kbar transition point. The later measurements (1968), as described by the authors of Reference 37, show a sudden increase (≈ 30%) in resistance at ~ 80 kbar, which is absent in the data of Fuller and Price [38].

The authors of Reference 37 suggest and discuss three possible causes of this resistance jump at approximately 80 kbars. Briefly, these suggested mechanisms are:

1. The $\alpha \rightarrow \varepsilon$ transition starts at a lower pressure than 130 kbars.
2. The shock creates lattice defects.
3. Part of the α – iron is transformed into a new phase under the influence of the very high shear stresses associated with the shock. This explanation was favored by the authors of Reference 37.

As shown in Figure 9, the predicted LDP initiation shock pressure (Ps_f = 86 kbars) is remarkably close to the shock pressure region (70 to 80 kbars) where the so–called 80 kbar resistance increase occurs. Consequently, it is strongly suspected that initial LDP is the reason for the resistance rise. LDP, if indeed it is occurring, could be responsible for any of the three causative mechanisms, or any combination of these mechanisms, which were mentioned above. LDP would certainly cause heterogenous lattice defects and could be responsible for partial $\alpha \rightarrow \varepsilon$ transformations and/or some other new transient phase as well.

LDP by definition implies lattice bond breaking, or scission, which is a lattice defect. When some (or all) of these broken bonds recombine after the shock passage, they may well combine in the ε lattice form. As the shock level (or particle velocity level) increases, it is certainly physically plausible that bond breaking and recombination in the ε – structure would intensify and even escalate to a complete $\alpha \rightarrow \varepsilon$ phase transformation.

This postulated LDP description for the iron $\alpha \rightarrow \varepsilon$ transformation is somewhat analogous to remarks made in Reference 1 with respect to shock–induced thermocouple re-

sponse and detonation of PBX–9404. The trend of the thermocouple response in shocked PBX–9404 and PMMA is similar to the trend of the resistance change in shocked iron [37]. That is, the electrical signal deviates from the expected values and escalates as Ps or Up is increased.

Consequently, Fitzgerald's LDP is suggested as a common triggering or causative mechanism behind the observed electrical signal behavior of these three diverse materials (PBX–9404, PMMA, and iron) under shock–loaded conditions.

It is also suggested that the electrical resistance of shocked iron be experimentally evaluated again ($40 \leq Ps \leq 180$ kbars) where ΔPs between data points is about 5 kbars in the region between 70 and 90 kbars. Shocked thermocouple output for these conditions would be of interest also.

3. NaCl

V_f, Us_f, and Ps_f were computed for S. C. NaCl, which was shock–loaded in the <100> direction. The Us versus Up relationship employed was from Reference 39 (Table 1). This relation (Us = 3.528 + 1.343 * Up km/sec) was a fit to Los Alamos Scientific Laboratory (LASL) data obtained at "low" pressures. A plot of this data in Figure 4 of Reference 39 reveals that <100> – cut S. C. samples were employed.

The C_L and C_t values, to compute C_s, were from Reference 40. An average value of m and d_1 was employed to compute V_1. This value of d_1 (2.82 Å) agrees rather closely with similar information given in textbook examples [41, pp. 652–655] for the NaCl crystal lattice structure. An average value of m(m_{AV}) is considered appropriate, since shock–loading it in the <100> direction would involve both Na and Cl atoms whose masses are not greatly different (Appendix A).

Utilizing the information described above and given in Tables 1 and 2, V_f and Ps_f for <100> cut S. C. NaCl was computed to be:

V_f = 0.253 km/sec

P_{sf} = 21.0 kbars

Reference 29 discusses the low–pressure (20 – 30 kbars) phase transition controversy with regard to NaCl. Royce [40] states that a "weak" transformation is observed at Ps_t = 29 kbars in <100> – cut S. C. NaCl. The two–wave velocities differed by only 1/2 to 1%, and rather sensitive quartz transducers must be employed to detect it. In Reference 42, Weidner and Royce conclude that "the 29 kbar discontinuity for 100 crystals can be considered a second HEL caused by strain hardening on the major slip system." The above Ps_f value (21 kbars) is indicative that LDP could begin a few kilobars below the observed Ps_t point, and, as such, also be the responsible mechanism.

Indicator lines for Ps_f and Ps_t are drawn in Figure 10 where shock–induced polarization maximum amplitude signals (volts) are plotted as a function of Ps. These test results are from Reference 43, Table 1. The specimens were <100> oriented single–crystals whose diameter was 25 mm. The specimen thickness, which influences the signal, varied as tabulated in Figure 10. This thickness variation is not enough to influence the trend of the signal output as a function of shock pressure. In particular, note the six–fold increase in signal amplitude from Ps = 16 kbars to Ps = 25 kbars. These specimens had essentially identical thicknesses, so there is

definitely not a thickness effect on the signal magnitudes. Obviously, the LDP Ps_f and its probable consequence, Ps_t, are remarkably close to the onset and step–like increase of the electrical polarization test signals.

4. DISCUSSION

In Reference 1 and the present study, a total of nine different explosives and four different inert materials have been investigated for possible LDP effects. This has been accomplished by computing V_f and Ps_f for these materials, and comparing Ps_f with the shock pressures where some type of shock–induced reaction is occurring. On the basis of these favorable comparisons it is suggested that the following shock–loaded material phenomena is explained by Fitzgerald's LDP–critical particle velocity, V_f, concept as applied to shocked solid substances:

1. Threshold detonation pressure, P_D, for explosives. That is, $P_D \sim Ps_f$. [1, this report].

2. Threshold detonation pressure, P_D, variation with density (ρ_o). [1, this report].

3. Roth's observation [45] that although P_D for explosives varied with density (ρ_o), the particle velocity where P_D occurred was essentially invariant (Table 5, Fig. 11).

4. Experimentally observed "heterogenous hot spots" in shocked explosives. [2, this report] The bond or lattice break–up is not always homogeneous, and will not necessarily occur all at once at the same time.

5. A "catastrophic shock" event occurring at low shock pressures where "bond scission" occurred. Such an event was suggested by Graham [26] to account for effects which have been observed from examining a large amount of experimental data. These effects (and the LDP assessment examples) are:

   a. Anomalous electrical behavior [1, this report].

   b. Increased chemical activity [this report].

   c. Polymorphic phase changes [this report].

In the discussion of item 3, Table 5 and Figure 11 were mentioned to illustrate that V_f is practically invariant for these energetic materials. Table 6 and Figure 12 were prepared for the inert materials considered in Reference 1 and the present study. V_f range indicators are also shown for the metallic element data given in Reference 2, Chapter 3, Table 3.1. All of these V_f values are somewhat less than one km/sec, which is indicative of relatively low Ps_f values, commensurate with item 5 above.

An important spin–off from the LDP investigations has been the results reported in Reference 6. This document clearly shows the important relationship between V_1 (the De Broglie particle velocity) and classic experimental HEL particle velocity, Up_{HEL}. Since the De Broglie velocity is important at EPSP HEL conditions, it is reasonable to assume that it applies to conditions where the particle velocity is greater than V_1 or Up_{HEL}. In fact, Fitzgerald's LDP V_f derivation is based on the premise that the De Broglie relation, $Up = h/(2md_1')$, must be satisfied for $V_1 \leq Up \leq V_f$.

The De Broglie relation must also be satisfied for Up >> V_f, where no more reverse motion of the lattice can occur, since its lattice bonding energy is depleted. Consequently, something has to occur (a polymorphic phase change, atomic spacing compression, melting, vaporization, or some other phenomena) so that Up = $h/(2md_1')$ is satisfied. The stiffened Hugoniot relationship (Us vs. Up) observed at the higher shock pressures (or high Up) for certain materials is perhaps indicative of the severe atomic spacing compression (d_1') requirements, which may apply only to " free atoms" and not to the bulk particles.

Quite frankly, the author is amazed at the "predictive power" of Fitzgerald's LDP V_f concept as applied in Reference 1 and the present investigation to shock–loaded solid materials. It would be rather difficult to devise a strictly empirical procedure to predict as well for so many diverse substances. In direct contrast to an entirely empirical procedure, the LDP V_f concept has a considerable amount of unconventional rationale behind it (reverse lattice motion via lattice bond cohesive energy utilization). The agreement between the LDP V_f predictions and the experimental reactive conditions for seventeen different cases can hardly be considered fortuitous.

Consequently, a "bottom line" result of this investigation is:

> The LDP V_f effect is strongly believed to provide a "common cause" or "trigger mechanism" for the relatively low–pressure shock–induced reactive behavior observed experimentally in certain solid materials.

5. RECOMMENDATIONS

Some recommendations for additional work have already been made, either explicitly or implicitly, in the previous sections. For easy reference, these are restated here.

A. The importance of the De Broglie momentum–wave length relation with respect to particle velocity propagation in shock–loaded solid materials is apparent from References 1, 6, 68, and the present report. The De Broglie relation implications should be addressed in future shock physics research, particularly via numerical CMD experimentation.

B. Additional available experimental shocked material data should be investigated for possible LDP V_f effects. Certain anomalous behavior observed at relatively low–level shock–loading could possibly be explained as a V_f effect, or as a V_1 effect [6, 68].

C. The electrical resistance of shocked iron should be experimentally evaluated again ($40 \leq Ps_f \leq 180$ kbars) where the ΔPs between data points is no greater than 5 kbars in the region between 70 and 100 kbars. Shocked thermocouple output for these conditions would also be desirable.

D. Additional experimentation (polarization, thermocouples, electrical resistance, etc.) should be performed on NaCl where Ps is varied from about 15 to 35 kbars in ΔPs increments no greater than 5 kbars.

TABLE 1. Shocked Material Information.

Material ~	ρ_o grams/cm^3	C_o cm/μ–sec	S ~	Source ~
PBX–9407	1.60 (pressed)	0.1328	1.993	[16]
Octol	1.803 (cast)	0.221	2.51	[9]
TNT	1.648 (pressed)	0.238	2.215	[14] averaged results
PETN	1.72 (pressed)	0.183	3.45	[17]
	1.778 (crystal)	0.274	1.81	[22]
Iron	7.84	0.463	1.33	[33, 34]
NaCl	2.165	0.3528 LASL Data Fit	1.343 LASL Data Fit	[39]
PPMI	1.425	Non–linear U_s versus U_p variation. (Fig. 6)		[26, 28]

TABLE 2. Compilation of V_1, C_s, V_f, Us_f, and Ps_f Results.

Material ~	m_{AV} grams*10^{-23}	d_{1AV} cm*10^{-8}	V_1 cm/μ–sec	C_l cm/μ–sec	C_t cm/μ–sec	C_s cm/μ–sec	V_f cm/μ–sec	U_{sf} cm/μ–sec	P_{sf} kbars
PBX–9407 ρ_o = 1.608	1.7840	2.2303	0.008327	0.1922 [9]	0.1260 [9]	0.1070	0.03430	0.2012	11.10
PBX–9407* ρ_o = 1.780	1.7840	2.1560	0.008614	0.3040 [9]	0.1700 [9]	0.1582	0.04148	0.2155 ρ_o=1.608 Rel.	15.91
Octol ρ_o = 1.80	1.7659	2.1407	0.008764	0.3140 [9]	0.1660 [9]	0.1601	0.04208	0.3266	24.74
TNT (P) ρ_o = 1.648	1.7959	2.2171	0.008321	0.2798 [14]	0.1384 [14]	0.1394	0.03847	0.3232	20.49
PETN ρ_o = 1.72	1.8102	2.1915	0.008352	0.2820 [17]	0.1480 [17]	0.1434	0.03903	0.3176	21.07
PETN ρ_o = 1.778	1.8102	2.1694	0.008437	See Table 3	See Table 3	0.1528	0.04037	0.3470	24.87
Iron ρ_o = 7.84	9.27 [2]	2.48 [2]	0.00144 [2]	0.5498 [44]	0.3847 [44]	0.3158	0.02197	0.4923	86.26
NaCl ρ_o = 2.165	4.8525	2.8195	0.002421	0.474 [40] <100> cut	0.241 [40] <100> cut	0.238	0.0253	0.3867	21.16
PPMI ρ_o = 1.425	1.6278	2.2521	0.009032	0.239 [26]	0.0985 [26]	0.1129	0.03677	0.2870 (Fig. 6)	15.13

* Us_f for PBX–9407 (ρ_o = 1.78 G/CC) was computed from data for ρ_o = 1.608 G/CC.

TABLE 3. Single Crystal PETN Elastic Wave Velocities [24].

X	Type Mode	Direction of Motion	C_x km/sec	C_x^2 $(km/sec)^2$
1	L	100	3.1140	9.6970
2	T	001	1.6841	2.8362
3	T	010	1.4893	2.2180
4	L	001	2.6167	6.8471
5	T	010	1.6822	2.8298
6	T	100	1.6822	2.8298
7	L	110	2.9308	8.5896
8	T	–110	1.8197	3.3113
9	T	001	1.6866	2.8541

$$\sum C_x^2 = 42.0034 \ (km/sec)^2$$

$$C_s^2 = \frac{\sum C_x^2}{18} = 2.3335 \ (km/sec)^2$$

C_s = 1.5276 km/sec via Eq. 7

L = Longitudinal wave, C_L

T = Transverse or shear wave, C_t

TABLE 4. Theoretical and Experimental Reactive Shock Information Tabulation.

Material	V_1, V_f, U_{sf} cm/μ–sec	P_{sf} kbars	Exp. Data kbars or cm/μ–sec	Exp. Data Item	Exp. Data Ref.	Remarks with Regard to Experimental Data
PBX–9407 ρ_o = 1.60 g/cc	0.008327 0.03430 0.2012	11.10	9.35	P_{MIN}	[16]	Average result from time and distance to detonation test data. See main text.
			17.00	P_{50}	[11]	SSGT 50% firing stimulus. (Fig. 2)
Octol ρ_o = 1.80 g/cc (cast)	0.008764 0.04208 0.3266	24.74	25.00	P_{50}	[11]	SSGT 50% firing stimulus of pressed octol. (Fig. 3).
			22.00	P_i	[10]	LSGT detonation threshold Ps. Cast 75.25 octol. ρ_o = 1.79 g/cc
TNT ρ_o = 1.648 g/cc (pressed)	0.008321 0.03847 0.3232	20.49	24.00	P_R	[15]	Reaction noted in impact test of pressed TNT. ρ_o = 1.648 g/cc
PETN ρ_o = 1.72 g/cc (pressed)	0.008352 0.03903 0.3176	21.07	17.0	P_D	[17]	Detonation observed. No detonation at 15.0 kbars in sample.
PETN ρ_o = 1.778 g/cc (crystal)	0.008437 0.04037 0.3470	24.87	42.6	P_D	[23]	Detonation observed.
			35.0	P_R	[23]	High level reaction observed.
			22.0	P_R	[23]	Some reaction observed.
PPMI ρ_o = 1.425 g/cc	0.009032 0.03677 0.2870	15.13	18.0	P_R	[27]	Cusp in U_s vs. U_p relation, plus start of shock–induced polarization.
Iron ρ_o = 7.84 g/cc	0.00144 0.02197 0.4923	86.26	70.0 to 80.0	P_R	[35]	Increase in electric resistance measurement. (Fig. 9).
			130.0	P_R	[30]	Phase transition observed.
NaCl ρ_o = 2.165 g/cc <100> cut single crystal	0.002421 0.0253 0.3867	21.16	16.0 to 25.0	P_R	[43]	Shock–induced electrical signal increase. (Fig. 10).
			29.0	P_{st}	[40]	Phase transition observed.

TABLE 5. Summary of LDP Assessment Results for Explosives.

Explosive	ρ_o (g/cc)	V_1 (km/sec)	V_f (km/sec)	Ps_f (kbars)
Octol	1.80	0.08764	0.4208	24.74
Comp–B3	1.70	0.08571	0.4170	26.59
PBX–9407	1.78	0.08614	0.4148	15.91
PBX–9404	1.842	0.08879	0.4109	26.16
Comp–B	1.70	0.08228	0.4077	25.16
PETN (S.C.)	1.778	0.08437	0.4037	24.87
H–6	1.75	0.07959	0.3903	23.87
PETN (P)	1.72	0.08352	0.3903	21.07
TNT (P)	1.648	0.08321	0.3847	20.49
TNT (P)	1.635	0.08299	0.3739	18.09
PBX–9407	1.608	0.08327	0.3430	11.10
Tetryl	1.70	0.07729	0.3411	17.00
Tetryl	1.50	0.07443	0.3340*	8.53*

V_{1AV} = 0.08302 km/sec

V_{fAV} = 0.3871 km/sec

(P) = Pressed

(S.C.) = Single Crystal

* Correction of V_f, Ps_f given in [1]

TABLE 6. Summary of LDP Results for Inert Materials.

Substance	ρ_o (g/cc)	V_1 (km/sec)	V_f (km/sec)	P_{sf} (kbars)
PMMA	1.18	0.1417	0.5157	21.0
PPMI	1.425	0.09032	0.3677	15.0
NaCl (S. C.)	2.165	0.02421	0.253	21.0
Iron	7.84	0.01441	0.2197	86.0
20 Metals [2]	~		0.072 to 0.655	~

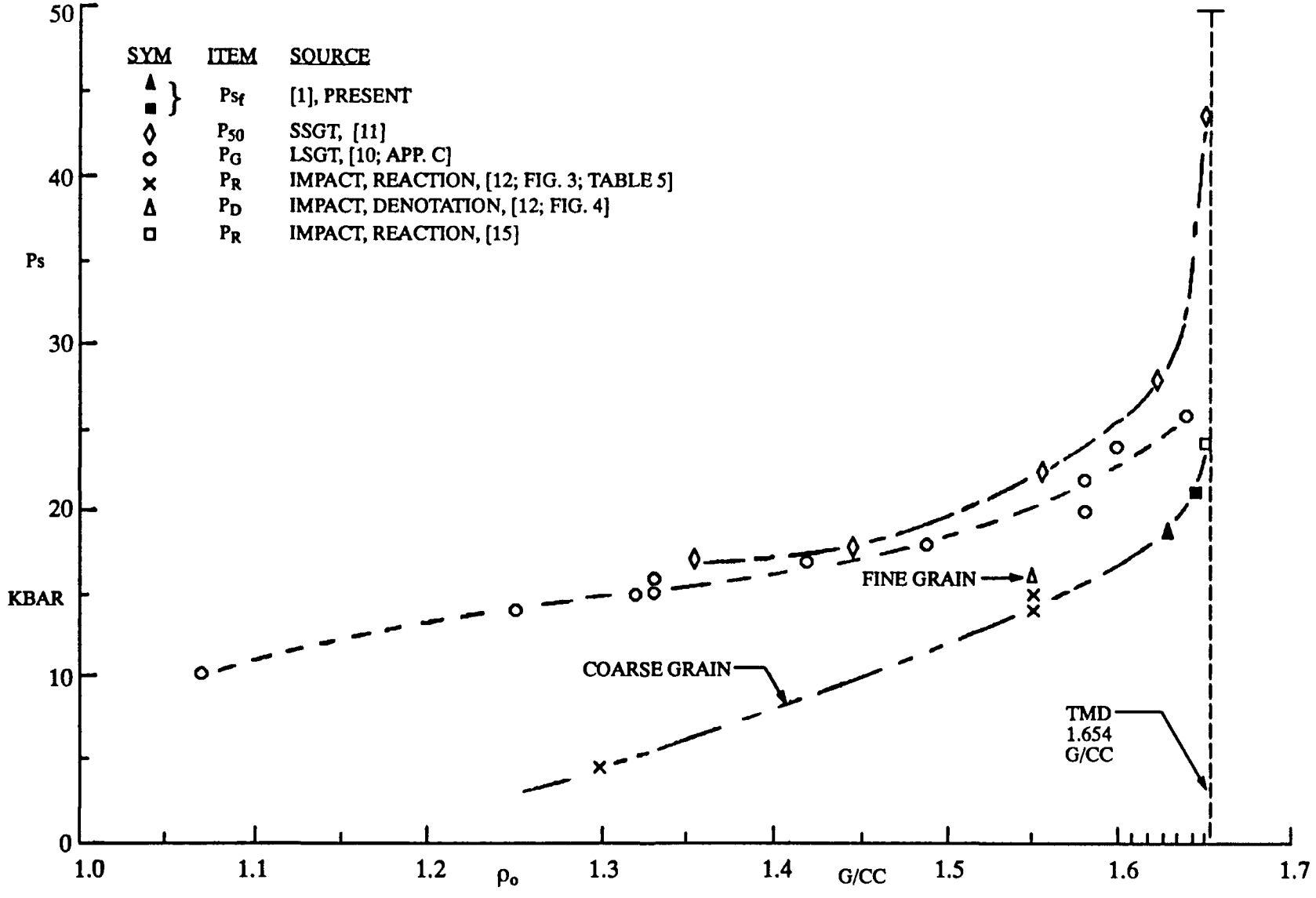

Figure 1. P_{Sf} Comparison with Test Results for Pressed TNT.

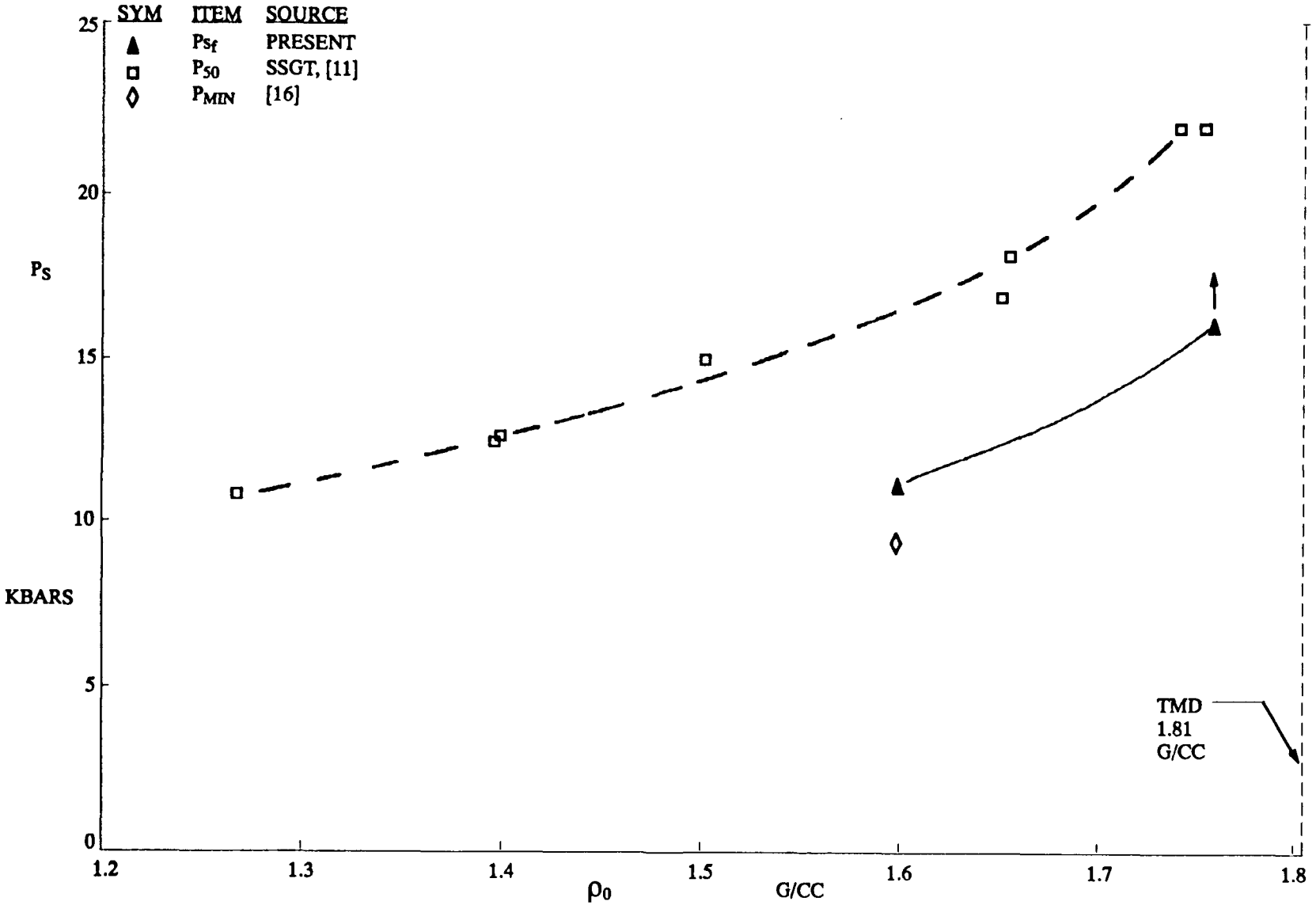

Figure 2. P_{sf} Comparison with Test Results for PBX–9407.

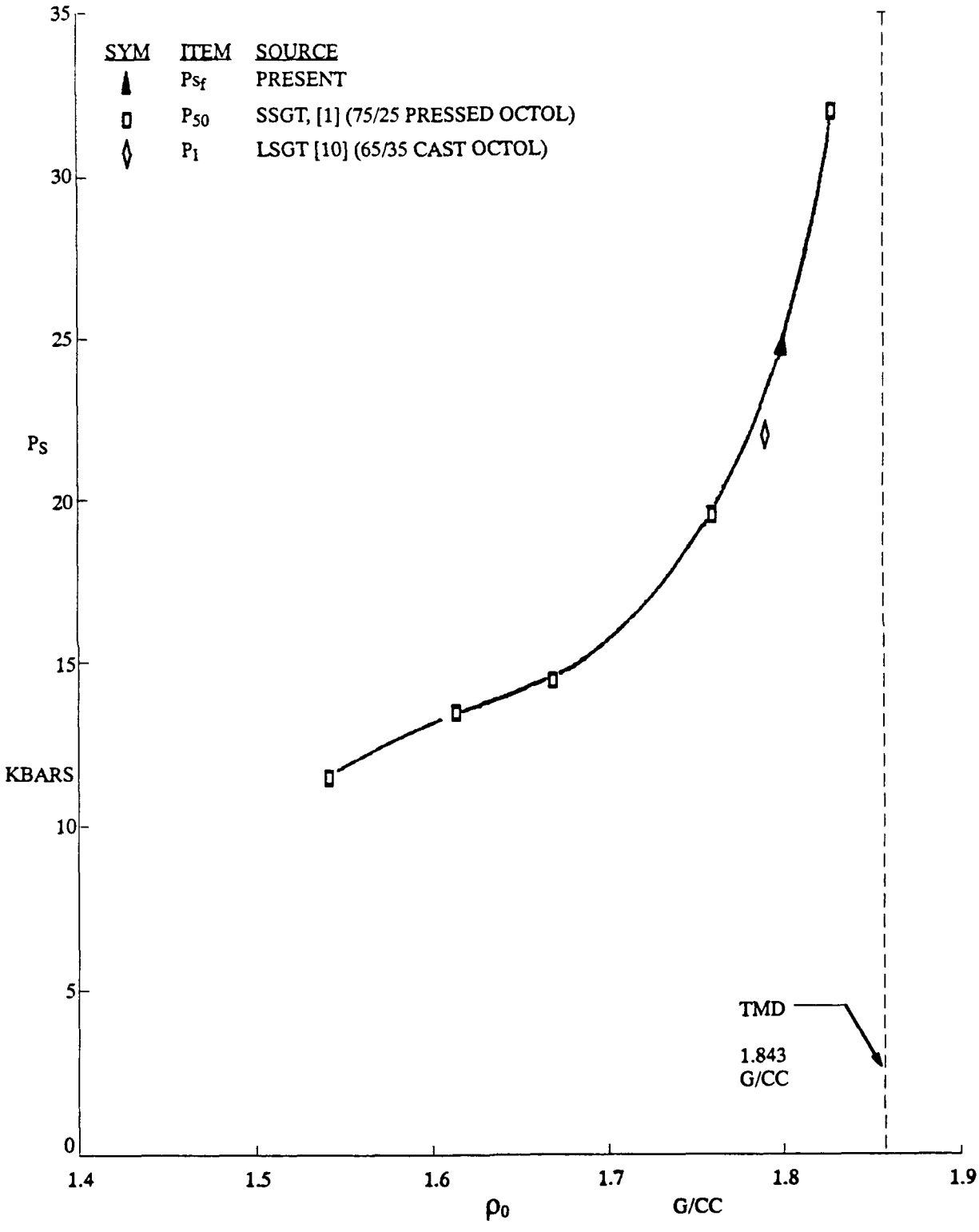

Figure 3. P_{sf} comparison with Test Results for Octol.

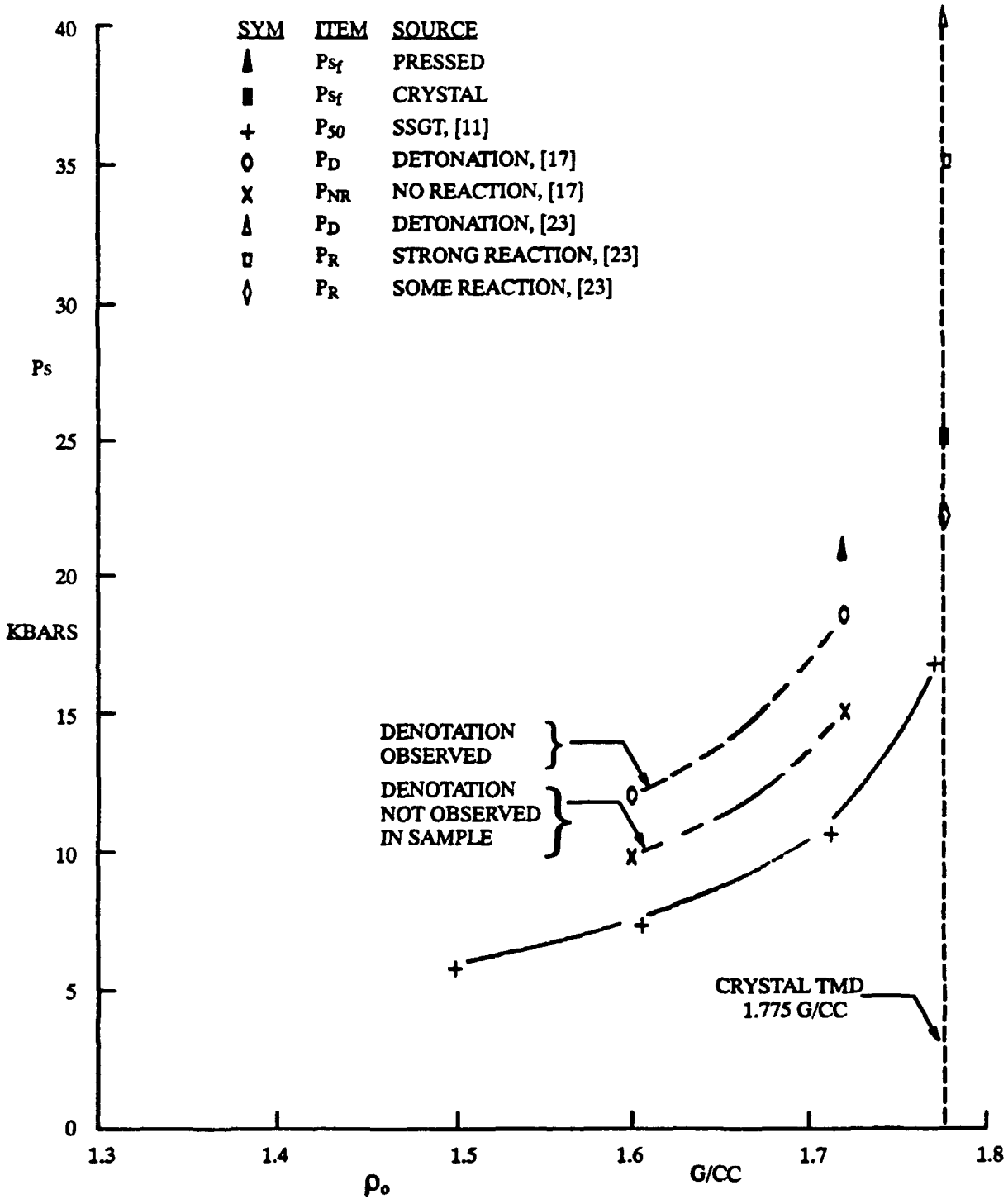

Figure 4. P_{sf} Comparison with Test Results for PETN.

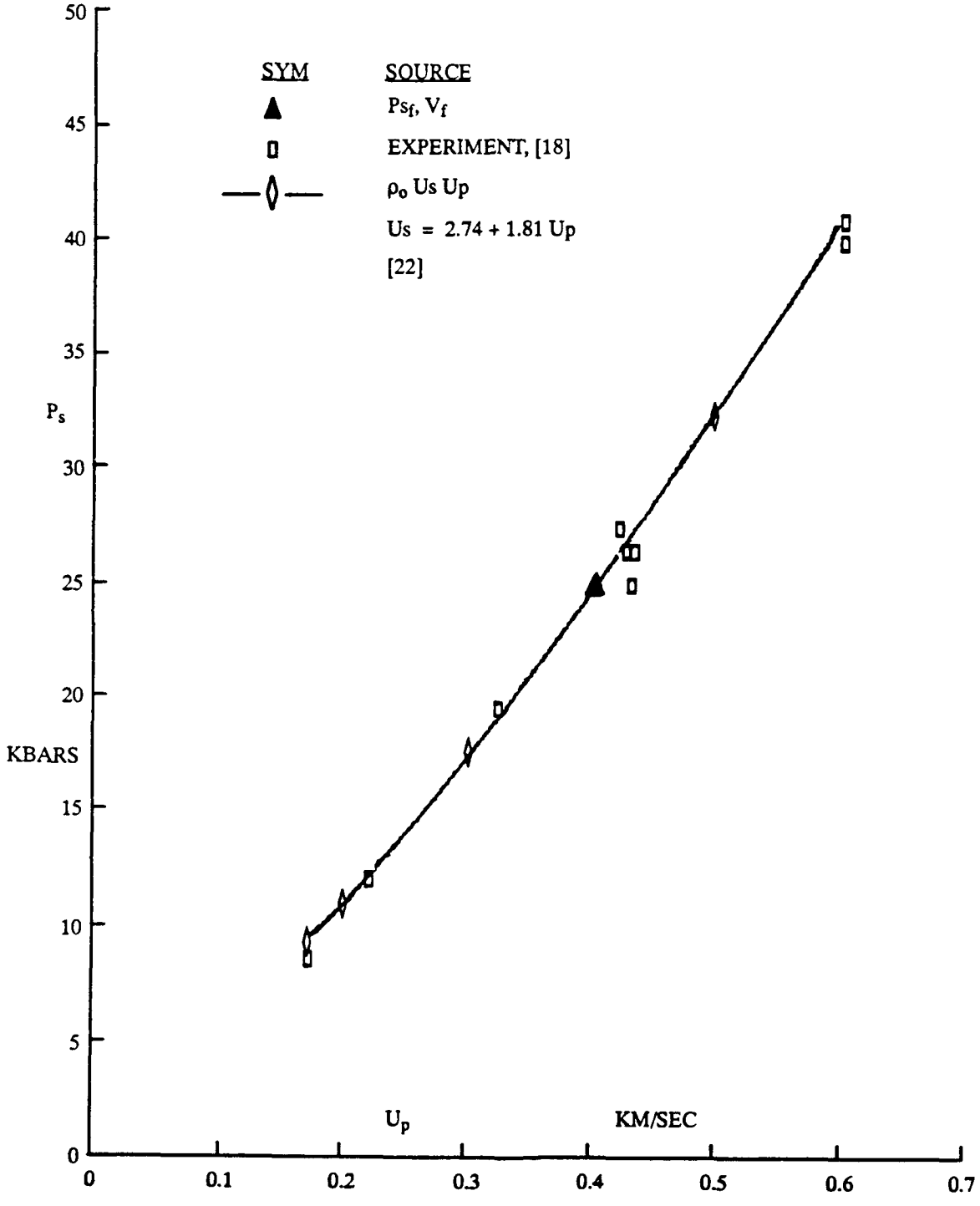

Figure 5. Ps Versus Up for <110> – Cut Single Crystal PETN.

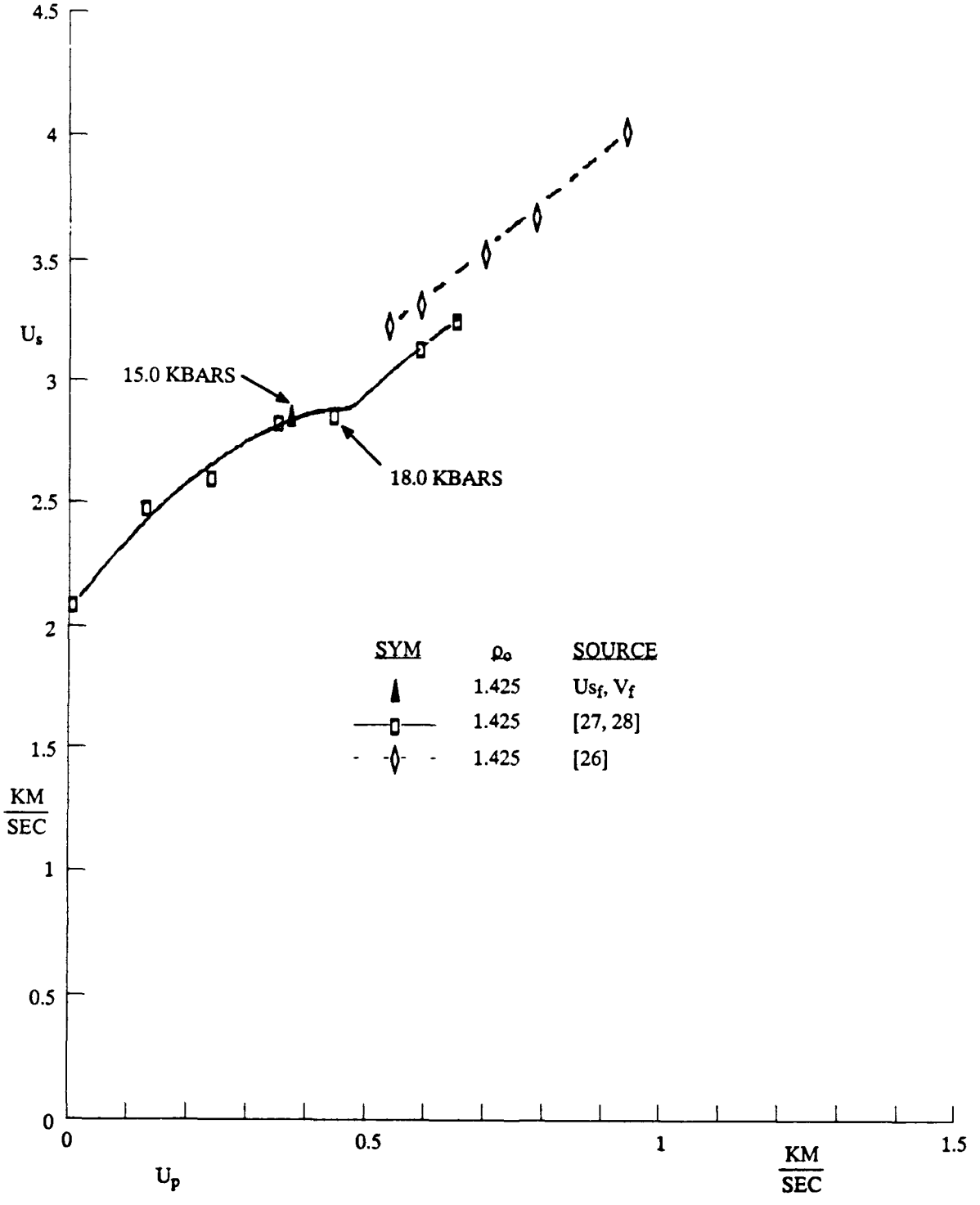

Figure 6. Us Versus Up for PPMI.

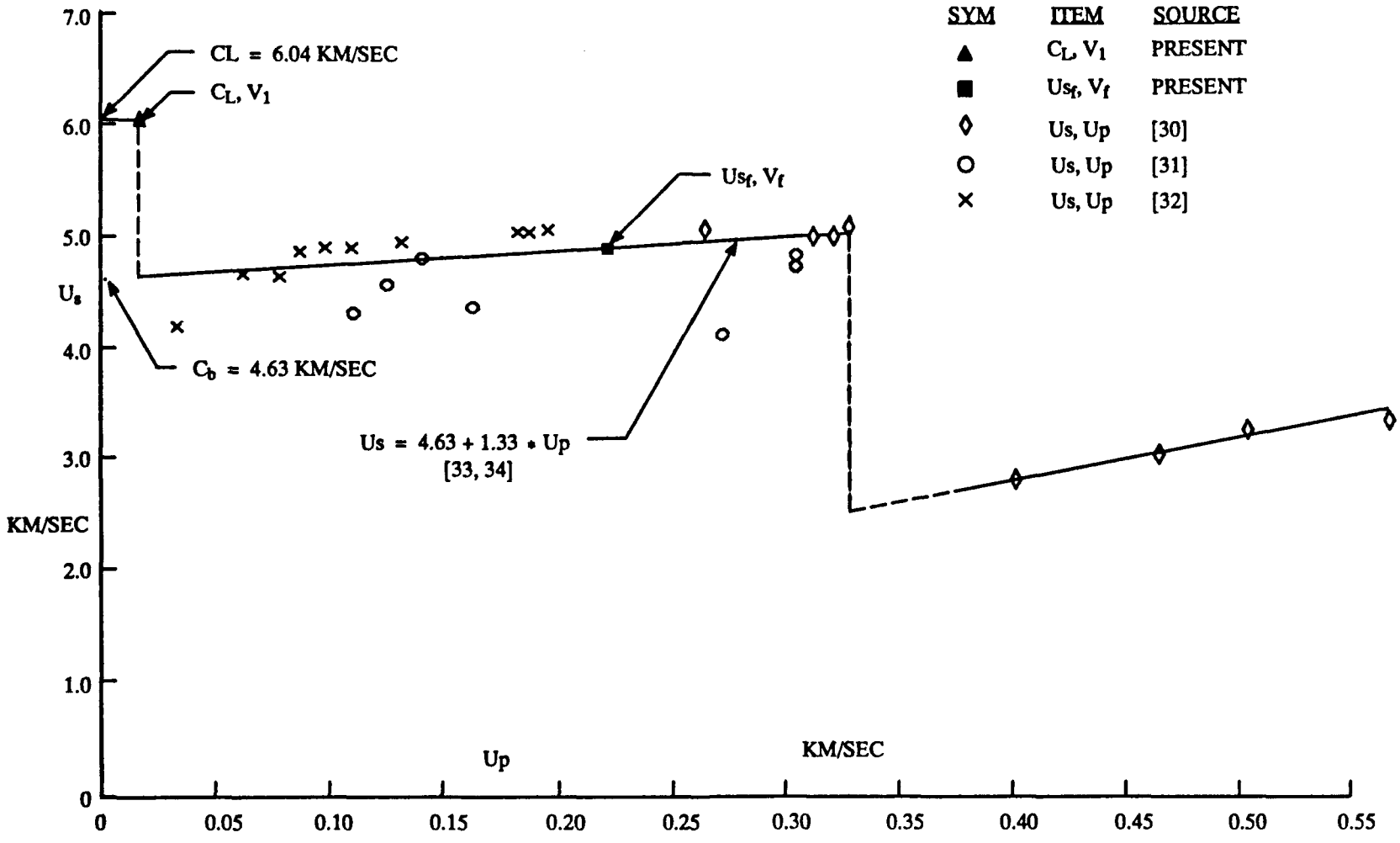

Figure 7. Us Versus Up for Iron.

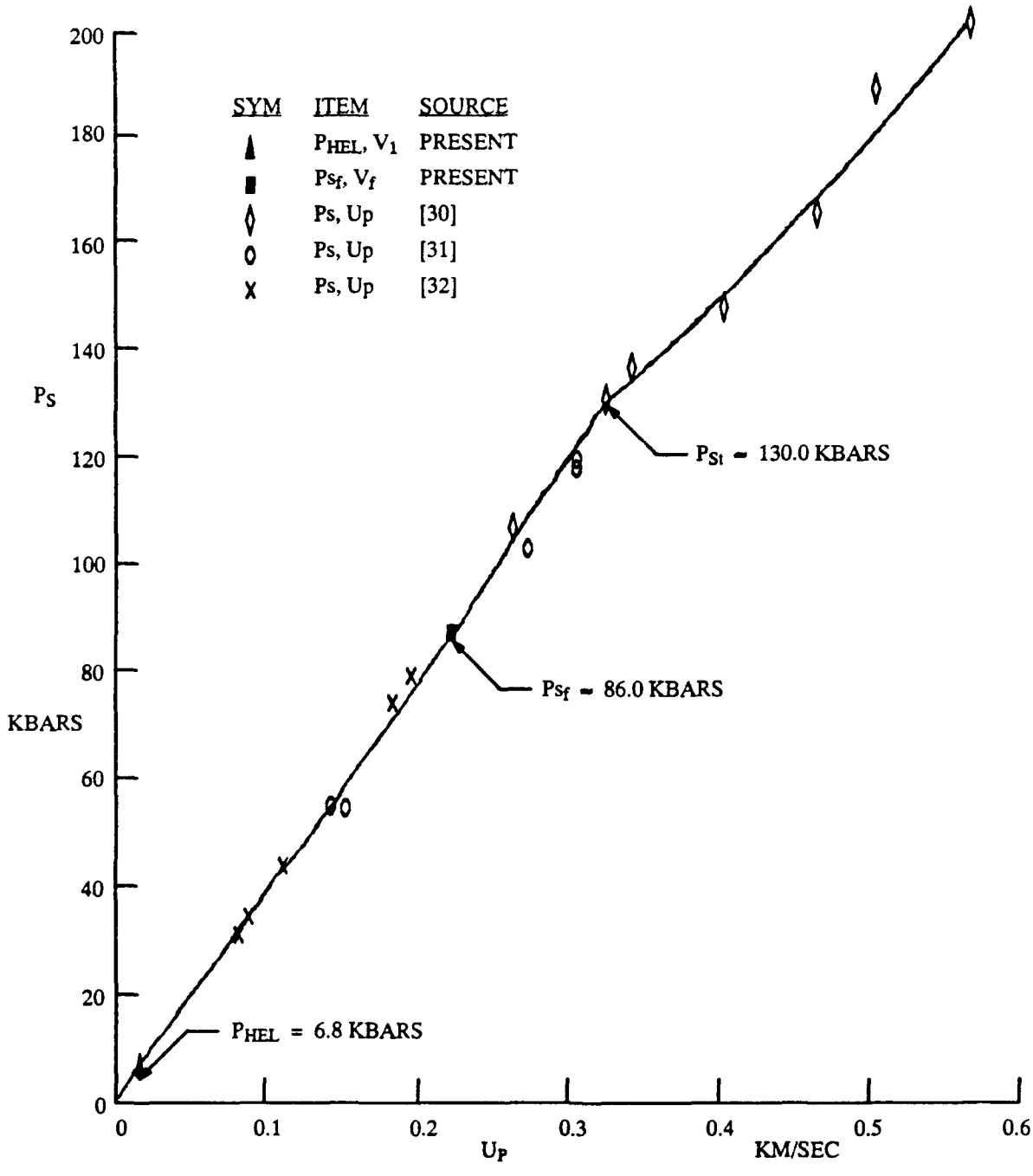

Figure 8. Ps Versus U_P for Iron.

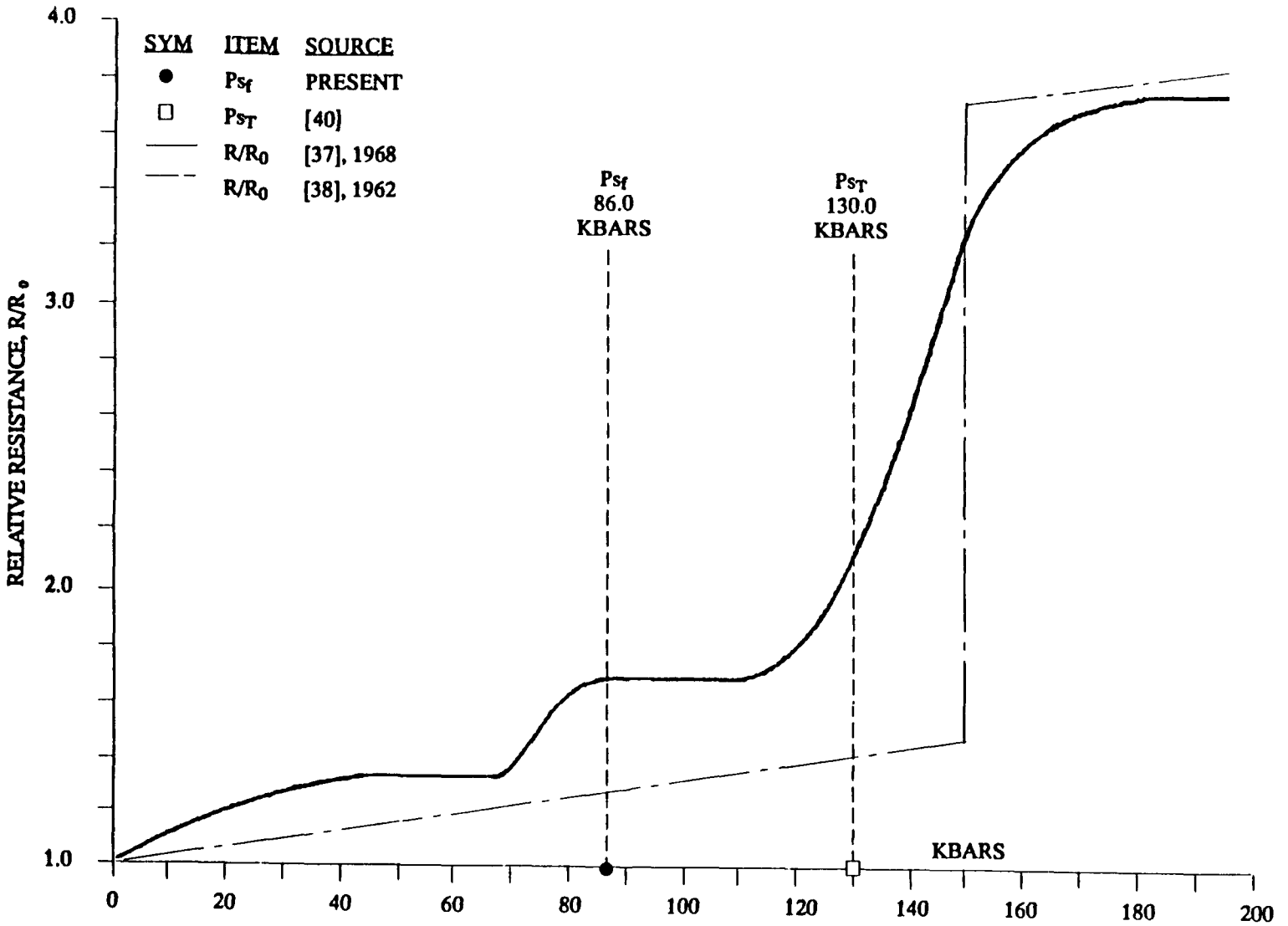

Figure 9. Relative Electrical Resistivity of Shocked Iron.

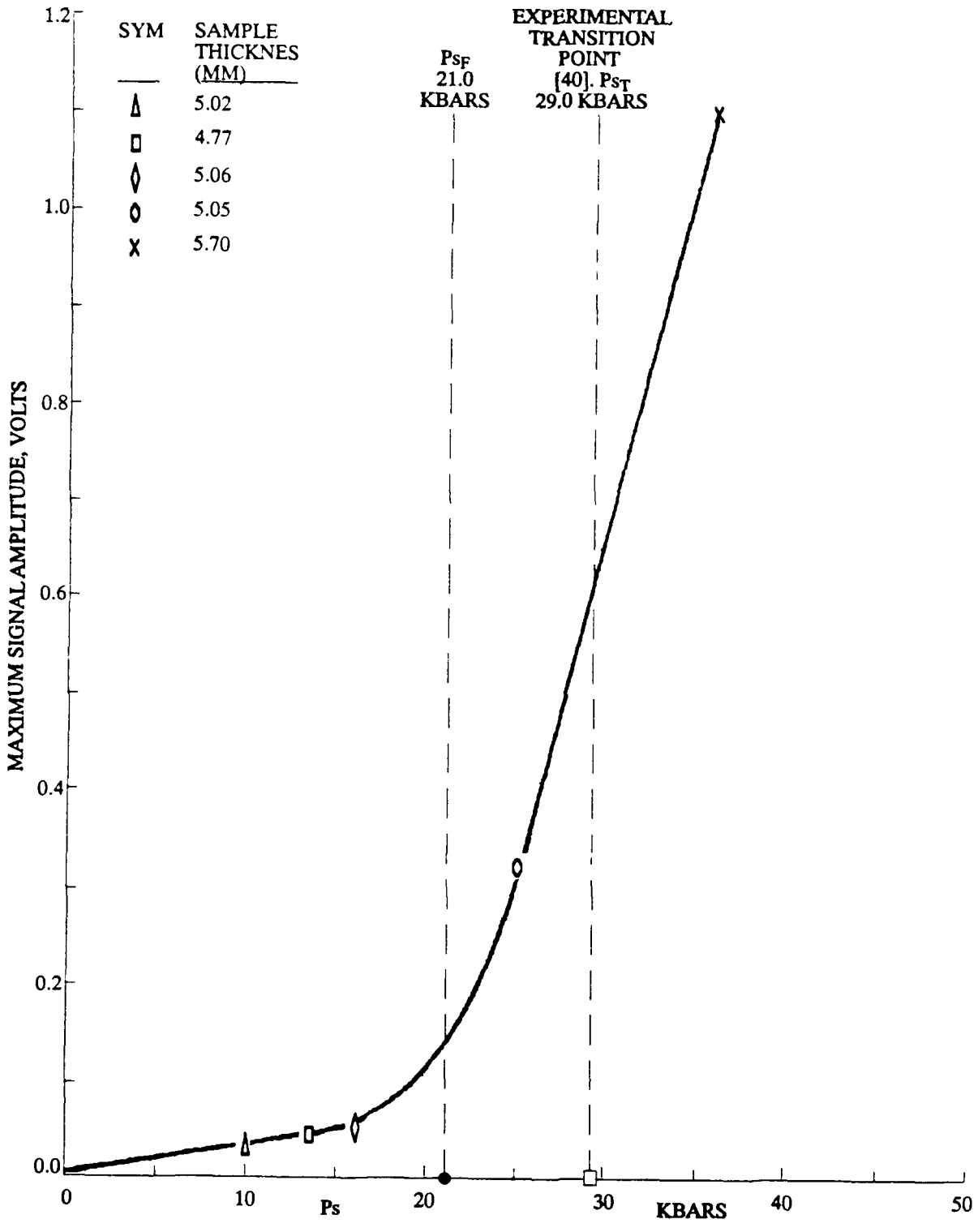

Figure 10. Maximum Signal Amplitude Versus Shock Pressure, Ps, from Polarization Tests of <100> Single-Crystal NaCl. [43, Table 1]

ITEM	ρ_0 (G/CC)
OCTOL	1.80
COMP-B3 [1]	1.70
PBX-9407	1.78
PBX-9404 [1]	1.842
COMP-B [1]	1.70
PETN (S.C.)	1.773
H-6 [1]	1.75
PETN (P)	1.72
TNT (P)	1.648
TNT (P) [1]	1.635
PBX-9407	1.608
TETRYL [1]	1.70
TETRYL [1]	1.50

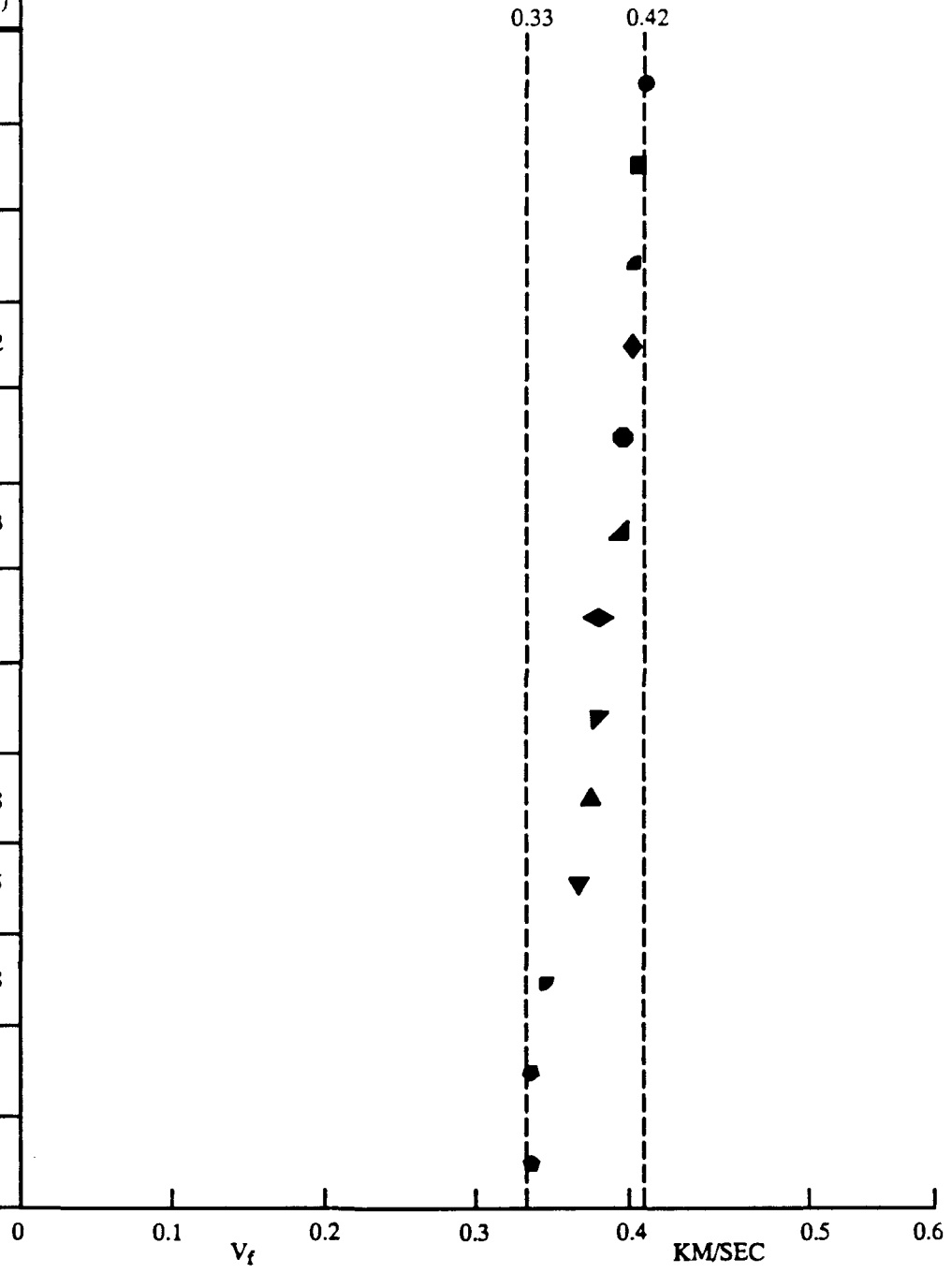

Figure 11. Predicted V_f for Diverse Energetic Materials.

ITEM	ρ_0 (G/CC)
PMMA	1.18
PPMI	1.425
NaCl	2.165
IRON	7.84
20 METALS [2]	~

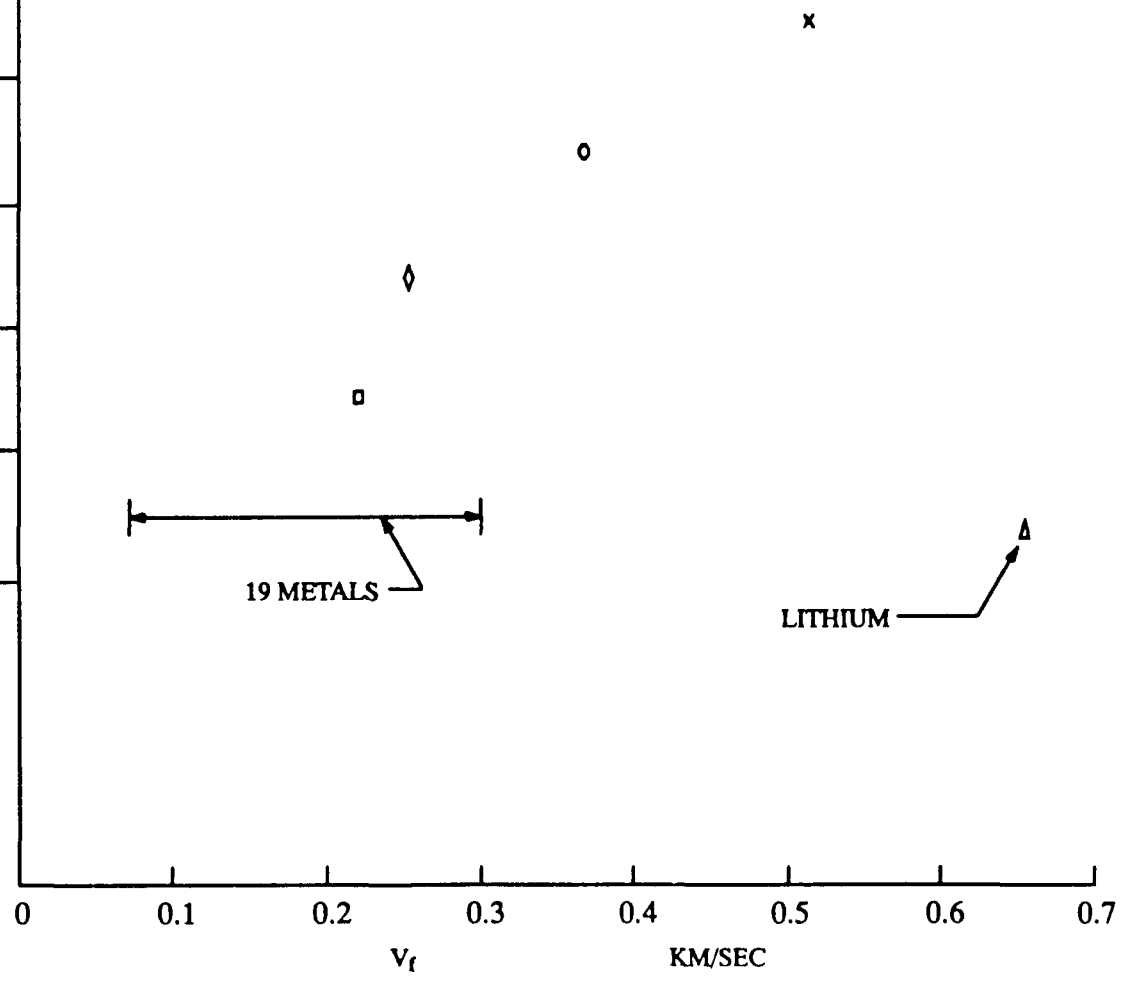

Figure 12. Predicted V_f for Diverse Inert Materials.

References

1. Billingsley, J. P., and Adams, C. L., "Application of Crystal Lattice Disintegration Criteria to Compute Minimum Shock Induced Reactive Conditions in Solid Explosives and Inert Materials." MICOM Technical Report RD–SS–89–10, March 1989. Aeroballistics Analysis Branch; Systems Simulation and Development Directorate; Research, Development, and Engineering Center, U.S. Army Missile Command, Redstone Arsenal, AL 35898.

2. Fitzgerald, E. R., Particle Waves and Deformation of Crystalline Solids, Interscience Publishers, a Division of John Wiley and Sons, Inc., New York, 1966.

3. Fitzgerald, E. R., and Wright, T. W., "Invariance of Sound Velocity Sums in Crystals." Article in Phys. Status Solid I, Vol. 24, 1967, pp. 37–44.

4. Fitzgerald, E. R., "Detonation in Crystalline Solids," Journal of Physics and Chemistry of Solids, Vol. 30, 1969, pp. 2771–2787.

5. McQueen, R. G.; Marsh, S. P.; Taylor, J. W.; Fritz, J. N.; and Carter, W. M., "The Equation of State of Solids from Shock Wave Studies," Hypervelocity Impact Phenomena, edited by Ray Kinslow, Academic Press, New York, 1970, pp. 293–417, and also Appendices A, B, C, D, and E of this book, pp. 515–568.

6. Billingsley, J. P., and Oliver, J. M., "The Relevance of the De Broglie Relation to the Hugoniot Elastic Limit (HEL) of Shock Loaded Solid Materials," MICOM Technical Report RD–SS–90–4, March 1990; Aeroballistics Branch; Systems Simulation and Development Directorate; Research, Development, and Engineering Center; U. S. Army Missile Command; Redstone Arsenal, AL 35898.

7. Walker, F. E., and Karo, A. M., "Comparison of Detonation Velocities and Average Vibrational Motion of Atom Pairs in Organic Explosives," Article in Shock Waves in Condensed Matter – 1987, edited by S. C. Schmidt and N. C. Holmes, published by Elsevier Science Publishers, B. V., 1988, pp. 543–546.

8. Owens, F. J. and Sharma, J., "X–Ray Photo Electron Spectroscopy and Paramagnetic Resonance Evidence for Shock Induced Intra Molecular Bond Breaking in Some Energetic Solids," Journal of Applied Physics, Vol. 51, No. 3, March 1980, pp. 1494–1497.

9. Dobratz, B. M., "LLNL Explosives Handbook, Properties of Chemical Explosives and Explosives Simulants," Report UCRL–52997, March 16, 1981. Lawrence Livermore National Laboratory, University of California, Livermore, CA 94550.

10. Price, D.; Clairmont, A. R. Jr.; and Erkman, J. O., "The NOL Large Scale Gap Test. III Compilation of Unclassified Data and Supplementary Information for Interpretation of Results." NOLTR–74–40 and AD–780 429; March 8, 1974; U. S. Naval Ordnance Laboratory; White Oak; Silver Spring, MD 20910.

11. Ayres, J. N.; Montesi, L. J.; and Bauer, R. J., "Small Scale Gap Test (SSGT) Data Compilation: 1959–1972 Vol. 1, Unclassified Explosives," NOLTR–73–132, Vol. I, October 26, 1973. Naval Ordnance Laboratory; White Oak; Silver Spring, MD 20910.

12. Taylor, B. C., and Ervin, L. W., "Separation of Ignition and Buildup to Detonation in Pressed TNT." paper presented at the Sixth International Symposium on Detonation; August 24–27, 1976; proceedings published as ONR–ACR–221; pp. 3–10; Office of Naval Research; Department of the Navy; Arlington, VA.

13. Wasley, R. J., Stress Wave Propagation in Solids; an Introduction, Marcel Dekker, Inc. New York, 1973.

14. Wasley, R. J., and Walker, F. E., "Dynamic Compressive Behavior of a Strain–Rate Sensitive, Polycrystalline, Organic Solid." Journal of Applied Physics, Vol. 40, No. 6, May 1969, pp. 2639–2648.

15. Wasley, R. J., and O'Brien, J. F., "Low–Pressure Hugoniots of Solid Explosives," paper presented at the Fourth International Symposium on Detonation; October 12–15, 1965; abstract in symposium proceedings published as ACR–126 by the office of Naval Research; Department of the Navy; Washington, DC.

16. Lindstrom, I. E., "Plane Shock Initiation of an RDX Plastic Bonded Explosive," Journal of Applied Physics; Vol. 37; No. 13; December, 1966; pp. 4873–4880.

17. Stirpe, D.; Johnson, J. O.; and Wackerle, J.; "Shock Initiation of XTX–8003 and Pressed PETN," Journal of Applied Physics, Vol. 41, No. 9, August 1970, pp. 3884–3893.

18. Halleck, P. M., and Wackerle, J., "Dynamic Elastic–Plastic Properties of Single–Crystal Pentaerythritol Tetranitrate," Journal of Applied Physics, Vol. 47, No. 3, March 1976, pp. 976-982.

19. Gibbs, T. R., and Popolato, A., editors of LASL Explosive Property Data. University of California, Berkeley; 1980, p. 318. (J. J. Dick, Reference 23, Attributes the S. C. PETN Data to B. G. Craig).

20. Dick, J. J., "Plane Shock Initiation of Detonation in γ–Irradiated Pentaerythritol Tetranitrate" Journal of Applied Physics, Vol. 53, No. 9, September 1982, pp. 6161–6167.

21. Dick, J. J., "Effect of Crystal Orientation on Shock Initiation Sensitivity of Pentaerythritol Tetranitrate Explosive," Applied Physics Letters, 44 (9), May 1, 1984.

22. Dick, J. J., "Pop Plot and Arrhenius Parameters for <110> Pentaerythritol Tetranitrate Single Crystals," paper in the proceedings of the fourth American Physical Society Topical Conference on Shock Waves in Condensed Matter; July 22–25, 1985; published as Shock Waves in Condensed Matter; edited by Y. M. Gupta, Plenum Press, New York, 1986, pp. 903–907.

23. Dick, J. J.; Pettit, D. R.; and Spencer, W. J.; "Crystal Orientation Effects in PETN Explosive with 4 G Pa Shocks," paper presented at the 1989 Topical Conference on Shock Compression of Condensed Matter; Albuquerque, New Mexico; August 14–17, 1989. Published as "Shock Compression of Condensed Matter – 1989," Ed. by S. C. Schmidt, J. N. Johnson, and L. W. Davidson, Elsievier Science Publishers, 1990.

24. Morris, C. E., "Adiabatic Elastic Moduli of Single Crystal Pentaerythritol Tetranitrate (PETN)." paper presented at the Sixth International Symposium on Detonation; August 24–27, 1976; proceedings published as ONR–ACR–221, pp. 396–402; Office of Naval Research; Department of the Navy; Arlington, VA.

25. Trotter, James, "Bond Lengths and Angles in Pentaerythritol Tetranitrate," ACTA Crysta Vol. 16, 1963. pp. 698–699.

26. Graham, R. A., "Shock Induced Electrical Activity in Polymeric Solids. A Mechanically Induced Bond Scission Model," The Journal of Physical Chemistry, Vol. 83, No. 23, 1979, pp. 3048–3056.

27. Sheffield, S. A., and Bloomquist, D. D., "Low Pressure Hugoniot Cusp in Polymeric Materials," article in AIP conference proceedings No. 78, entitled Shock Waves in Condensed Matter – 1981, edited by W. J. Nellis, L. Seaman, and R. A. Graham, published by the American Institute of Physics (AIP), 1982, pp. 57–61.

28. Personal Communication with Dr. S. A. Sheffield, August 31, 1989, at the Ninth International Detonation Symposium, Portland, OR.

29. Duvall, G. E., and Graham, R. A., "Phase Transitions Under Shock Wave Loading," Review of Modern Physics, Vol. 49, No. 3, July 1977, pp. 523–579.

30. Bancroft, D.; Peterson, E. L.; and Minshall, S.; "Polymorphism of Iron at High Pressures," Journal of Applied Physics, Vol. 27, No. 3, March 1956, pp. 291–298.

31. Hughes, D. S.; Gourley, L. E.; and Gourley, M. F.; "Shock Wave Compression of Iron and Bismuth," Journal of Applied Physics, Vol. 32, No. 4, April 1961, pp. 624–629.

32. Taylor, J. W., and Rice, M. H., "Elastic–Plastic Properties of Iron," Journal of Applied Physics, Vol. 34, No. 2, February 1963, pp. 364–371.

33. Barker, L. M., and Hollenbach, R. E., "Shock Study of the $\alpha \Leftrightarrow \varepsilon$ Phase Transition in Iron," Journal of Applied Physics, Vol. 45, No. 11, November 1974, pp. 4872–4887.

34. Barker, L. M., "α – Phase Hugoniot of Iron," Journal of Applied Physics, Vol. 46, No. 6, June 1975, pp. 2544–2547.

35. Minshall, F. S., "The Dynamic Response of Iron and Iron Alloys to Shock Waves," article in Response of Metals to High Velocity Deformation, proceedings of a Technical Conference; July 11–12, 1960; edited by P. G. Shewmon and V. F. Zackay; published by Interscience Publishers, Inc.; New York; 1961; pp. 249–272. (Also see the discussion of this paper pp. 272–274.)

36. Duvall, G. E., "Some Properties and Applications of Shock Waves," article in Response of Metals to High Velocity Deformation; proceedings of a Technical Conference; July 11–12, 1960; edited by P. G. Shewmon and V. F. Zackay; published by Interscience Publishers, Inc.; New York; 1961; pp. 165–202. (Also see the discussion of this paper pp. 202–203.)

37. Wong, J. Y.; Linde, R. K.; and De Carli, P. S.; "Dynamic Electrical Resistivity of Iron: Evidence for a New High Pressure Phase," Nature; Vol. 219; August 17, 1968; pp. 713–714.

38. Fuller, P. J. A., and Price, J. H., "Electrical Conductivity of Manganin and Iron at High Pressures," Nature; Vol. 193; January 20, 1962; pp. 262–263.

39. Hauver, G. E., and Melani, A.,"The Shock Hugoniot of Single–Crystal Sodium Chloride," U. S. Army Ballistics Research Memorandum No. 2061; August 1970; Aberdeen Proving Ground, Maryland.

40. Royce, E. B., "On the Low Pressure Phase Transition in NaCl," Lawrence Radiation Laboratory; Livermore, California; Report UCID–15454; January 1969.

41. Daniels, F., and Alberty, R. A., Physical Chemistry, John Wiley and Sons, Inc., New York, 1966.

42. Weidner, D. J., and Royce, E. B., "Yield Behavior of Shock–Compressed NaCl," Lawrence Radiation Laboratory, Livermore, California; Report UCID–15629; May 1970.

43. Linde, R. K.; Murri, W. J.; and Doran, D. G., "Shock–Induced Electrical Polarization of Alkali Halides," Journal of Applied Physics, Vol. 27, No. 7, June 1966, pp. 2527–2532.

44. American Institute of Physics Handbook, Dwight E. Gray, Coordinating editor, 2nd edition, McGraw–Hill Book Company, Inc., New York.

45. Roth, J., "Shock Sensitivity and Shock Hugoniots of High–Density Granular Explosives," paper in the Fifth International Symposium on Detonation; August 18–21, 1970; proceedings published as ARC–184; pp. 219–230; Office of Naval Research; Department of the Navy; Arlington, Virginia.

46. McQueen, R. G., and Marsh, S. P., "Ultimate Yield Strength of Copper," Journal of Applied Physics, Vol. 33, No. 2, February 1962, pp. 654–665.

47. Rodean, H. C., "Relationship for Condensed Materials Among Heat of Sublimation, Shock–Wave Velocity, and Particle Velocity," Journal of Chemical Physics, Vol. 49, No. 9, November 1968, pp. 4117–4127.

48. Rodean, H. C., "Relationship for Liquids Among Heat of Vaporization, Shock Wave Velocity, and Particle Velocity," Journal of Chemical Physics, Vol. 54, 1971, pp. 2280–2281.

49. Rodean, H. C., "Evaluation of Relations Among Stress Wave Parameters and Cohesive Energy of Condensed Materials," Journal of Chemical Physics, Vol. 61; No. 11; December 1, 1974; pp. 4848–4859.

50. Pastine, D. J. and Piacesi, D., "The Existence and Implications of Curvature in the Relation Between Shock and Particle Velocities for Metals," Journal of Physics and Chemistry of Solids, Vol. 27, 1966, pp. 1783–1792.

51. Otpushchennikov, N. F., "Speed of Sound and Heat of Sublimation for Metals," Soviet Physics Journal, No. 3, May–June 1965, pp. 20–23.

52. Nemilov, S. V., "Relationship Among the Velocity of Sound, the Mass of Atoms, and the Chemical Interaction Energy in Solids," article in Chemical Bonds in Solids, edited by N. N. Sirota, (Consultants Bureau, New York, 1972) Vol. 2, pp. 128–133 (translation of the proceedings of the International Sympoosium on Chemical Bonds in Semiconducting Crystals, Minsk, U. S. S. R., 1967).

53. Darwent, B. DeB., "Bond Dissociation Energies in Simple Molecules," National Bureau of Standards publication NSRDS–NBS–31; January 1970; Washington, DC 20402.

54. Grimvald, G., Thermophysical Properties of Materials, North–Holland Physics Publishing, Amsterdam, 1986.

55. Fitzgerald, E. R., "Particle Waves and Phonon Fission in Crystals," Physics Letters, Vol. 10; No. 1; May 15, 1964; pp. 42–43.

56. Zhurkov, S. N., "Kinetic Concept of the Strength of Solids," International Journal of Fracture Mechanics, Vol. 1, 1965, pp. 311–323.

57. Krausz, A. S., and Eyring, H., Deformation Kinetics, John Wiley and Sons, New York, 1975.

58. Grimvald, G. and Sjödin, S., "Correlation of Properties of Materials to Debye and Melting Temperatures," Physica Scripta, Vol. 10, 1974, pp. 340–352.

59. Holtzman, A. H., and Cowan, G. R., "The Strengthening of Austenitic Manganese Steel by Plane Shock Waves," article in Response of Metals to High Velocity Deformation, edited by P. G. Shewmon and V. F. Zackay, Interscience Publishers, New York, 1961, pp. 447–482.

60. Pugh, J. W.; Rose, R. M.; Paul, I. L.; and Radin, E. L.; "Mechanical Resonance Spectra in Human Cancellous Bone, Science, Vol. 181; No. 4096; July 20, 1973; pp. 271–272. Also, comments on this article by J. Black immediately following on page 273.

61. Fitzgerald, E. R., "Calcium–Isotope Effects in Mechanical Spectra of Cancellous Bone," Medical and Biological Engineering, September 1975, pp. 717–719.

62. Pugh, J. W., and Steiner, G. C., "Relationship Between the Structure and Mechanical Resonance Spectra in Cancellous Bone," Medical and Biological Engineering, September 1975, pp. 714–716.

63. Lambrakos, S.G., Peyrard, M., and Oran, E. S., "Molecular Dynamics Simulation of the Effect of Molecular Dissociation and Energy Absorption on Denotation Structure in Solids," Paper No. 142 in Vol. III preprints of papers presented at The Ninth Symposium (International) on Denotation, Aug, 28 – Sept. 1, 1989, pp. 812–819.

64. Lambrakos, S. G., Oran, E.S., Boris, J. P., and Guiguis, R. N., "Molecular Dynamics Simulation of Shock Induced denotations in Energetic Solids," Article in Shock Waves in Condensed Matter – 1987, Ed. by S. C. Schmidt and N. C. Holmes, Elsevier Science Publishers B.V. 1988, pp. 499–502.

65. Karo, B. M., Walker, F. E., Deboni, T. M., and Hardy, J. R., "The Simulation of Shock Induced Energy Flux in Molecular Solids," Article in Dynamics of Shock Waves, Explosions, and Denotations, ed. by J. R. Bowen, N. Mason, A. R. Oppenheim, and R. I. Soloukin, Progress in Astronautics and Aeronautics, Vol. 94, 1984, Martin Summerfield, Ed–in–chief, pp. 405–415.

66. Trevino, S. F. and Tsai, D. H., "Simulation of the Initiation of Denotation in an Energetic Molecular Crystal: The Overdriven Case," Article in preceeding of The Eighth Symposium (International) on Denotation, July 15 – 19, 1985, pp. 870–877.

67. Dremin, A. N., Klimenko, V. Y., Davidova, O. N., and Zoludeva, T. A., "Multiprocess Denotation Model," Paper No. 159 in Vol. I of the preprints of paper presented at the Ninth Symposium (International) on Denotation, Aug. 28 – Sept. 1, 1989, pp. 287–291.

68. Billingsley, J. P. and Oliver, J. M., "The Relevance of the De Broglie Velocity ($V_1 = h/2md_1$) to Shock Loading Induced Reactions in Lead Azide," MICOM Technical Report RD–SS–_____ (to be published), Aeroballistics Analysis, System Simulation and Development Directorate, Research, Develoment, and Engineering Center, U. S. Army Missile Command, Redstone Arsenal, Alabama 35898.

69. Rice, M. H., "Penetration of High Explosives by Inert Projectiles," Report No. SSS–R–78–3512, November, 1977, System Science and Software, P. O. Box 1620 La Jolla, California, 92038.

70. Dunn, J. E., "Implication and Origins of Shock Structure in Solids," Paper in Shock Compression of Condensed Matter – 1989, Ed. by S. C. Schmidt, J. N. Johnson, and L. W. Davison, Elsevier Science Publishers B.V. 1990, pp. 21–32.

APPENDIX A

COMPUTATION OF M_{AV} AND D_{1AV} FOR CHEMICAL COMPOUNDS AND MIXTURES OF COMPOUNDS

APPENDIX A

COMPUTATION OF M_{AV} AND D_{1AV} FOR CHEMICAL COMPOUNDS AND MIXTURES OF COMPOUNDS

Certain solid materials considered in this study were either chemical compounds (PETN, PPMI, and NaCl), or mixtures of chemical compounds. For these compounds and/or mixtures, the weighted average mass, m_{av}, of a single atom in the material was desired.

First, it was necessary to compute the mass of a single atom for each of the elements contained in the solid. Each solid was composed of one or more, but not all, of the following elements:

Carbon, C; Hydrogen, H; Nitrogen, N;

Oxygen, O; Sodium, Na;

Chlorine, Cl; Flourine, F.

The mass of a single atom of these elements is:

$$m = \frac{MW}{N_{av}} = \frac{\text{Grams/Gram-Mole}}{\text{Atoms/Gram-Mole}} = \frac{\text{Grams}}{\text{Atom}} \qquad \text{(A-1)}$$

Where:

$$MW = \text{Molecular Weight, } \frac{\text{Grams}}{\text{Gram-Mole}}$$

$$N_{av} = \text{Avogadros Number} = 6.02252 \times 10^{+23} \frac{\text{Atoms}}{\text{Gram-Mole}}$$

Table A–1 lists MW and m for each of the elements in the above list. Values of N_{av} and MW are from various chemistry text books and handbooks.

To compute the average weight (m_{av}) of an atom in the material, the chemical formula or proportional chemical composition is required. Of course, the weight (m) of each elemental atom must also be known, since m_{av} is just a weighted average of the elemental atoms in the material.

When m_{av} is computed, then the average space between atoms (d_{1av}) is given by the following relation:

$$d_{1av} = \left(\frac{m_{av}}{\varrho_o}\right)^{1/3} = \text{cm} \qquad \text{(A-2)}$$

Computations of m_{av} and d_{1av} for PBX–9407, octol, PETN, PPMI, and NaCl are included in this appendix.

TABLE A–1. Mass of a Single Atom for Selected Elements.

Element	MW	N_{av}	m
–	Grams / Gram–Mole	Atoms / Gram–Mole	Grams / Atom
Carbon, C	12.011	$6.02252(10^{23})$	$1.9943(10^{-23})$
Hydrogen, H	1.008	$6.02252(10^{23})$	$0.1674(10^{-23})$
Nitrogen, N	14.008	$6.02252(10^{23})$	$2.3259(10^{-23})$
Oxygen, O	16.00	$6.02252(10^{23})$	$2.6567(10^{-23})$
Chlorine, Cl	35.45	$6.02252(10^{23})$	$5.8874(10^{-23})$
Flourine, F	18.99	$6.02252(10^{23})$	$3.1546(10^{-23})$
Sodium, Na	28.99	$6.02252(10^{23})$	$3.8173(10^{-23})$

PBX–9407:

ρ_o = 1.608 grams/cm^3

Chemical composition: $C_{1.41}\ H_{2.66}\ N_{2.54}\ O_{2.54}\ Cl_{0.07}\ F_{0.09}$

$C_{1.41}$: $1.41 * 1.9943(10^{-23}) = 2.8120(10^{-23})$ grams

$H_{2.66}$: $2.66 * 0.1674(10^{-23}) = 0.4453(10^{-23})$ grams

$N_{2.54}$: $2.54 * 2.3259(10^{-23}) = 5.9078(10^{-23})$ grams

$O_{2.54}$: $2.54 * 2.6567(10^{-23}) = 6.7480(10^{-23})$ grams

$Cl_{0.07}$: $0.07 * 5.8874(10^{-23}) = 0.4121(10^{-23})$ grams

$F_{0.09}$: $0.09 * 3.1546(10^{-23}) = 0.2839(10^{-23})$ grams

9.31 atoms $16.6091(10^{-23})$ grams

$$m_{AV} = \frac{16.6091(10^{-23})}{9.31} = 1.7840(10^{-23})\ \frac{\text{grams}}{\text{atom}}$$

$$d^3_{1AV} = \frac{m_{AV}}{\rho_o} = \frac{17.840(10^{-24})}{1.608} = 11.0945(10^{-24})\text{cm}^3$$

$$d_{1AV} = 2.2303(10^{-8})\text{cm}$$

Octol

ρ_o = 1.80 grams/cc

Chemical composition: $C_{1.78}\ H_{2.58}\ N_{2.36}\ O_{2.69}$ (75% HMX, 25% TNT)

$C_{1.78}$:	$1.78 * 1.9943(10^{-23})$	$= 3.5499(10^{-23})$ grams
$H_{2.58}$:	$2.58 * 0.1674(10^{-23})$	$= 0.4319(10^{-23})$ grams
$N_{2.36}$:	$2.36 * 2.3259(10^{-23})$	$= 5.4891(10^{-23})$ grams
$O_{2.69}$:	$2.69 * 2.6567(10^{-23})$	$= 7.1465(10^{-23})$ grams
	9.41 atoms	$16.6174(10^{-23})$ grams

$$m_{AV} = \frac{16.6174(10^{-23})}{9.41} = 1.7659(10^{-23})\ \frac{\text{grams}}{\text{atom}}$$

$$d_{IAV}^3 = \frac{m_{AV}}{\rho_o} = \frac{17.6592(10^{-24})}{1.80} = 9.8107(10^{-24})\text{cm}^3$$

$$d_1 = 2.1407(10^{-8})\text{cm}$$

Pentaerythritol Tetranitrate (PETN)

ρ_o = 1.773 grams/cc

Chemical composition: $C_5\ H_8\ N_4\ O_{12}$

C_5:	$5 * 1.9943(10^{-23})$	$= 9.9715(10^{-23})$ grams
H_8:	$8 * 0.1674(10^{-23})$	$= 1.3392(10^{-23})$ grams
N_4:	$4 * 2.3259(10^{-23})$	$= 9.3036(10^{-23})$ grams
O_{12}:	$12 * 2.6567(10^{-23})$	$= 31.8804(10^{-23})$ grams
	29 atoms	$52.4947(10^{-23})$ grams

$$m_{AV} = \frac{52.4947(10^{-23})}{29} = 1.8102(10^{-23})\ \frac{\text{grams}}{\text{atom}}$$

$$d_{IAV}^3 = \frac{m_{AV}}{\rho_o} = \frac{18.102(10^{-24})}{1.773}\ \frac{\text{grams}}{\left(\frac{\text{grams}}{\text{cm}^3}\right)} = 10.2098 * (10^{-24})\ \text{cm}^3$$

$$d_{IAV} = 2.1694(10^{-8})\ \text{cm}$$

Polypyromellitimide (PPMI)

ρ_o = 1.425 grams/cc

Chemical composition [26]: $(C_{22}\ H_{10}\ N_2\ O_5)_N$

C_{22}:	22.0 * 1.9943 (10^{-23})	=	43.8746 (10^{-23}) grams
H_{10}:	10.0 * 0.1674 (10^{-23})	=	1.6740 (10^{-23}) grams
N_2:	2.0 * 2.3259 (10^{-23})	=	4.6518 (10^{-23}) grams
O_5:	5.0 * 2.6567 (10^{-23})	=	13.2835 (10^{-23}) grams
	39.0 atoms		63.4839 (10^{-23}) grams

$$m_{AV} = \frac{63.4839\ (10^{-23})}{39.0} = 1.6278\ (10^{-23})\ \frac{\text{grams}}{\text{atom}}$$

$$d_{1AV}^3 = \frac{m_{AV}}{\rho_o} = \frac{16.278\ (10^{-24})}{1.425} = 11.4231\ (10^{-24})\ \text{cm}^3$$

$$d_{1AV} = 2.2521\ (10^{-8})\ \text{cm}$$

Sodium Chloride

ρ_o = 2.165 grams/cc

Chemical Composition: N_aC_L

Na:	1.0 * 3.8173 (10^{-23})	=	3.8173 (10^{-23}) grams
Cl:	1.0 * 5.8874 (10^{-23})	=	5.8874 (10^{-23}) grams
	2.0 atoms		9.7047 (10^{-23}) grams

$$m_{AV} = \frac{9.7047\ (10^{-23})}{2.0} = 4.8525\ (10^{-23})\ \text{grams}$$

$$d_{1AV}^3 = \frac{m_{AV}}{\rho_o} = \frac{48.525\ (10^{-24})}{2.165} = 22.4127\ (10^{-24})\ \text{cm}^3$$

$$d_{1AV} = 2.8195\ (10^{-8})\ \text{cm} \approx 2.82\ (10^{-8})\ \text{cm}$$

This value for d_1 agrees well with the atomic separation distance for NaCl given in Reference 41, pages 652 through 655, as a textbook example.

APPENDIX B

RELATIONSHIPS BETWEEN ELASTIC WAVE VELOCITIES AND THE COHESIVE ENERGY OF SOLID MATERIALS

APPENDIX B

RELATIONSHIPS BETWEEN ELASTIC WAVE VELOCITIES AND THE COHESIVE ENERGY OF SOLID MATERIALS

Since the publication of Reference 1 and in the latter part of this investigation, some important technical literature [46 through 49] was discovered which relates the shock wave and particle velocity parameters (C_o and S in Eq. 1) to the material cohesive energy. This relationship, which was suggested by McQueen and Marsh [46], has been thoroughly investigated by Rodean [47, 48, 49]. The relation, employed by Rodean in his extensive comparisons of experimental data, is:

$$\frac{1}{2}\left(\frac{C_o}{S}\right)^2 = E_c \qquad \text{(B–1)}$$

or

$$C_o^2 = 2S^2 E_c$$

where

$C_o \approx C_b$ = bulk sound velocity = $\sqrt{K/\rho_o}$

K = bulk modulus, gram $(cm/sec)^2$

E_c = material cohesive energy per unit mass, ergs/gram or $(cm/sec)^2$.

≈ H_s, sublimation energy per unit mass, ergs/gram or $(cm/sec)^2$.

Note that:

$$E_c = \frac{U_c}{AW} \text{ or } \frac{U_c}{MW} = \frac{D}{m} \qquad \text{(B–2)}$$

where:

U_c = cohesive energy per molecular weight (MW, grams) of a compound or atomic weight (AW, grams) of an element

= $N_{AV} D$ for elements

= $C_A N_{AV} D$ for compounds or mixtures

D = cohesive energy per atom, gram $(cm/sec)^2$

m = mass of an atom for elements or average mass of an atom for compounds and mixtures, grams

$AW = N_{AV} m$ = atomic weight, grams

$MW = C_A N_{AV} m$ = molecular weight, grams

N_{AV} = Avogadro's number [Appendix A]

C_A = constant for a given compound or element

Since S ~ 1.4 ~ $\sqrt{2}$ for many materials, then Equation B–1 becomes approximately

$$\frac{C_b^2}{4} \approx E_c = \frac{D}{m} \qquad \text{or} \qquad C_b \approx 2\sqrt{E_c} = 2\sqrt{D/m} \tag{B–3}$$

Rodean provides extensive comparative results for Equation B–1 (56 metals, 12 compounds, and 4 polymers).

The general concept that the cohesive energy of a solid is related to the bulk sound wave velocity is not new, dating prior to World War I. Rodean [47] cites recent developments contained in References 50 and 51. Otpushchennikov [51] develops the following relation which is also derived in a number of solid state physics textbooks.

$$C_b^2 = \frac{m_1\, n_1}{9} E_c = \frac{m_1\, n_1}{9} \frac{D}{m} \tag{B–4}$$

where m_1 and n_1 are exponents in the potential energy relation. Otpushchennikov employed $m_1 * n_1 = 45$ to make his comparisons with experimental data ($C_b^2 = 5\, E_c$).

Rodean [49] notes that $m_1\, n_1 = 32$ would provide a better fit to the data. If $m_1\, n_1 = 36$, then Equation B–4 is equivalent to Equation B–3.

In Reference 49, Rodean discusses the results of Nemilov [52] who derived the following relation between C_t, the shear wave velocity, and the cohesive energy, E_c.

$$C_t^2 = E_c = \frac{D}{m} \tag{B–5}$$

Nemilov presented comparative results for 17 elemental metals and two compounds which agreed very well with Equation B–5. He also presented data for certain elements and compounds where:

$$C_t^2 = 2\, E_c = \frac{2\, D}{m} \tag{B–6}$$

For SiO_2 (glass) and alkali halide compounds, Nemilov's comparative results indicated that:

$$C_t^2 = \frac{E_c}{2} = \frac{D}{2m} \tag{B–7}$$

However for the alkali halides, Nemilov actually employed E_b (binding energy required to transform the solid to an ionized gas) instead of E_c (cohesive energy, energy required to transform the solid to an un–ionized or neutral gas). If E_c is employed for these alkali halides, then Equation B–5 is satisfied rather well as shown by the comparative results in Table B–1. The values of U_c for the alkali halides in Table B1 are from Reference 53 where they are called the dissociation energy. In these cases, $E_b \sim 2\ E_c$.

Grimvald [54, pg. 1] points out that the binding energy, E_b, may be different from the cohesive energy, E_c, particularly for ionic solids. He also cautions that the distinction between the binding energy and cohesive energy is not always made in the literature. Rodean [49] comments on the important distinction between E_c and E_b.

It is noteworthy that Fitzgerald [55] in 1964 had also suggested Equation B–5 and presented comparative results for 12 metals. That is, in Reference 55, C_s was the shear wave velocity and was favorably compared to $\sqrt{D/m}$ for metals. Later, by 1966 [2], Fitzgerald had derived the relation for C_s utilized in the main body of this report (Eq. 6) which is:

$$C_s^2 = \frac{C_L^2 + 2\,C_t^2}{6} \qquad \text{(B–8)}$$

This is essentially a weighted average of the sum of the squares of the wave velocities for isotropic materials. A somewhat more general result for certain anisotropic materials is given by Equation 7 [3, for additional comments on the implications of the general C_s definition].

For many materials, C_s as defined by Equation B–8 is practically equal to C_t [1, Table 2; this report, Table 2]. This explains the good agreement with $\sqrt{D/m}$ for both C_s and C_t, where data for the same elemental metals were compared.

It is also interesting that both C_s and C_t are approximately equal to C_D, the average sound velocity employed in Debye's theory of specific heats. That is:

$$C_D \sim C_T \sim C_S \qquad \text{(B–9)}$$

Grimvald [54] provides the following relations for C_D:

$$\frac{3}{C_D^3} = \frac{1}{C_L^3} + \frac{2}{C_t^3} \qquad \text{(B–10)}$$

$$C_D = C_T\left\{\frac{2}{3} + \frac{1}{3}\left[\frac{1 - 2\nu}{2\,(1 - \nu)}\right]^{3/2}\right\}^{-1/3} = (1.12 \pm 0.02)\,C_T \qquad \text{(B–11)}$$

$$\text{If } \nu = 0.31 \pm 0.14$$

where ν is Poisson's ratio, which is approximately 0.31 for many solid materials.

C_D is compared to $\sqrt{D/m}$ in Table B–1 for 16 alkali halide compounds where C_D was computed via Equation B–11. Values of C_s and C_t also are shown in Table B–1 for some of these materials. Similar comparative information for polymethyl methacrylate (PMMA) and iron is also presented in Table B–1. The value of U_c for PMMA is from Reference 56 by Zhurkov. Zhurkov's results are mentioned by Krausz and Eyring [57] in their discussion of the rate theory of fracture (Chapter 4, Section 4.4).

Grimvald [54] notes that C_D can be related to the Debye temperature, θ. He and Sjödin [58] provide a correlation of cohesive energy and Debye temperature data for a variety of materials.

The information from different sources cited in this Appendix clearly indicates that $\sqrt{D/m}$ is related to the velocity of sound or elastic wave propagation (C_b, C_t, C_s, and C_D) in materials. C_t, C_s, and C_D are approximately equal in magnitude. C_b is usually somewhat larger than C_t, C_s, and C_D.

In the present report and in Reference 1, C_s was employed in the LDP analysis as a measure of $\sqrt{D/m}$ for substances (primarily energetic materials) where the cohesive energy was somewhat uncertain, particularly under shock–loading circumstances. If C_t or C_D had been employed for V_{Lf} in Equation 8, the V_f results would be essentially the same.

If C_b had been utilized for V_{Lf} in Equation 8 to compute V_f, then V_f, U_{sf} and P_{sf} would generally be larger than the results given herein and in Reference 1. Note that V_f is approximately equal to the geometric mean value of V_1 and V_{Lf}.

$$V_f \approx \sqrt{V_1} * \sqrt{V_{Lf}} \approx \sqrt{V_1} * \sqrt[4]{E_c} \qquad \text{(B–12)}$$

Thus V_f is not extremely sensitive to small changes in V_{Lf} or E_c.

From the comparative results presented herein (Section III, A) and in Reference 2, it is believed that C_s^2 (or even C_t^2 or C_D^2) is a good measure of the cohesive energy for energetic materials. This belief is strengthened by the estimates of the energy per gram (E'_s = D/m) necessary for complete vaporization of Comp–B and PBX–9404 which was found in Reference 69. This information is listed in Table B–2 along with Ct, C_D, C_s for these explosives. Note that $\sqrt{E'_s}$ compares reasonably well with these elastic wave velocities for both explosives.

From the information given in Table B–3 and plotted in Figure B–1, it appears that C_b^2 is a good measure of the heat of detonation (ΔH_{DET}) of energetic materials. That is, this information indicates that:

$$C_b^2 \approx \Delta H_{DET} = \frac{\Delta h_{DET}}{m_{Av}} \qquad \text{(B–13)}$$

where:

ΔH_{DET} = Heat of Detonation, Mega Joules/Kilogram or $(km/sec)^2$.

The values of C_b and ΔH_{DET} in Table B–2 are from Reference 9.

TABLE B–1. Comparison of Elastic Wave Velocities and Cohesive Energy for Selected Inert Materials.

Compound	MW	U_c	Uc/MW or D/m	$\sqrt{U_c/MW}$ or $\sqrt{D/m}$	Ct	C_D	C_s
~	grams	gram $(cm/sec)^2 * 10^{-10}$	$(cm/sec)^2 * 10^{-10}$	km/sec	km/sec	km/sec	km/sec
Cs Br	212.8	381.0	1.790	1.330	1.16	1.30	
K Br	119.0	382.8	3.217	1.793	1.695	1.90	
K Cl	74.6	427.0	5.7239	2.392	1.77 [44]	1.99	2.09
K F	58.1	494.0	8.5026	2.916	2.59	2.90	
K I	166.0	331.0	1.9939	1.412	1.47	1.65	
Li Br	86.9	423.0	4.8677	2.206	2.07	2.32	
Li Cl	42.4	469.0	11.0613	3.326	3.06	3.43	
Li F	25.9	577.0	22.2780	4.720	4.88 [44]	5.46	3.87
Li I	133.9	351.0	2.6214	1.619	1.61	1.80	
Na Br	102.9	366.1	3.5568	1.886	1.81	2.03	
Na Cl	58.5	410.0	7.0085	2.647	2.41 [40]	2.70	2.38
Na I	149.9	297.0	1.9813	1.408	1.51	1.69	
Rb Br	165.4	385.0	2.3277	1.526	1.39	1.56	
Rb Cl	120.9	444.0	3.6725	1.916	1.66	1.86	
Rb F	104.5	490.0	4.6890	2.165	2.13	2.39	
Rb I	212.4	331.0	1.5584	1.248	1.17	1.31	
Iron	55.9	415.3 [52]	7.429	2.726	3.85 [44]	4.31	3.16
PMMA	97.1	221.8 [56]	2.2842	1.51	1.373 [1]	1.54	1.36

U_c data from Reference 53, except as noted.
Ct data from Reference 52, except as noted.

TABLE B–2. Comparisons of Elastic Wave Velocities and Estimates of Vaporization Energy per Gram for Comp–B and PBX–9404.

EXPLOSIVE	ρ_o	E'_s	E'_s	$\sqrt{E'_s}$	Ct	C_D	C_s
-	GRAM/CC	ERGS/GRAM	$(KM/SEC)^2$	KM/SEC	KM/SEC	KM/SEC	KM/SEC
		[69]			[9]	Eq. B–11	[1]
COMP–B	1.72	$3.00 * 10^{10}$	3.00	1.732	1.71	1.92	1.61
PBX–9404	1.84	$3.25 * 10^{10}$	3.25	1.803	1.57	1.76	1.49

TABLE B–3. Comparison of Elastic Wave Velocities and Heat of Detonation for Selected Energetic Materials.

Substance	ΔH_{DET} MJ/KG	ΔH_{DET} $(km/sec)^2$	$\sqrt{\Delta H_{DET}}$ km/sec	C_b km/sec	C_s km/sec
Comp–B3	4.69(E)	4.69	2.166	2.42	1.612
Comp–B	5.86(C)	5.86	2.421	2.42	1.612
PETN	5.73(E)	5.73	2.394	2.32	1.582
PBX–9407	6.11(C)	6.11	2.472	2.32	1.070
PBX–9404	5.36(E)	5.36	2.315	2.26	1.491
TNT(P)	4.27(E)	4.27	2.066	2.08	1.310
TETRYL	4.56(E)	4.56	2.135	1.76	1.165
TAT B	4.52(C)	4.52	2.126	1.44	1.000
Octol	5.98(C)	5.98	2.445	2.49	1.601
RDX	5.94(E)	5.94	2.437	2.65	~
PBX–9501	6.03(C)	6.03	2.455	2.50	~
PBX–9011	5.69(C)	5.69	2.385	2.41	~
PBX–9010	5.69(C)	5.69	2.385	2.13	~
LX–17	4.27(C)	4.27	2.066	2.04	~

(P) – Pressed

(C) – Calculated

(E) – Experimental

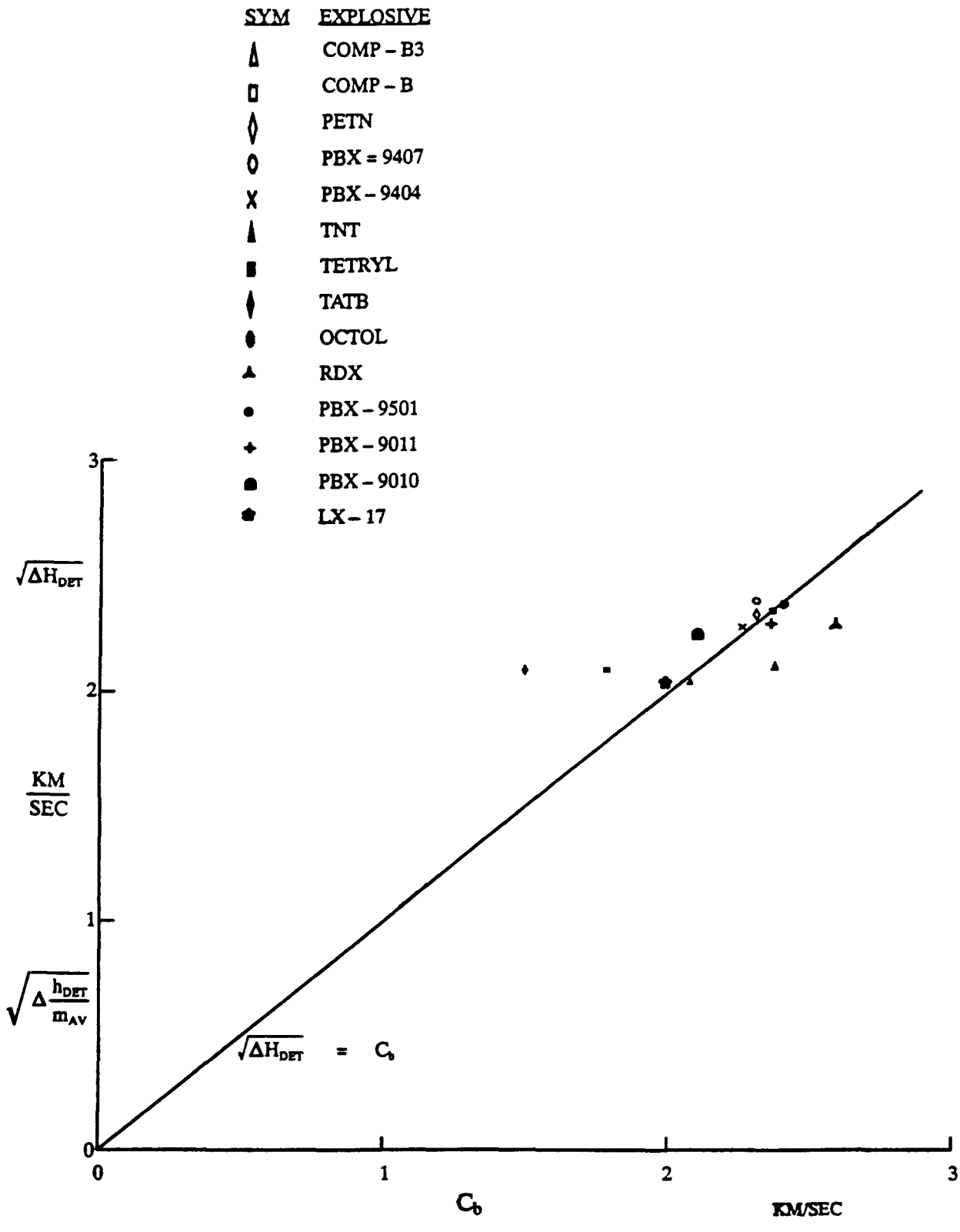

Figure B–1. ΔH_{DET} or $\frac{\Delta h_{DET}}{m_{AV}}$ Versus C_b.

APPENDIX C

CALCIUM ATOM EFFECTS ON BONE VIBRATION RESONANT FREQUENCIES

APPENDIX C

CALCIUM ATOM EFFECTS ON BONE VIBRATION RESONANT FREQUENCIES

In certain bio–mechanics investigations with vibrating bone segments [60], it was found that the frequency relation given by Fitzgerald [2, Chapter II] was the one that fit the data. This frequency relation is:

$$\nu_m = \left(\frac{h}{8\ m\ S^2}\right) n^2 \qquad \text{(C–1)}$$

where

h = Planck's Constant

m = Mass of the atom responsible for the resonance frequency

s = Repetitive segment length of the structure

n = integer, n = 1, 2, 3, etc.

The resonant frequencies were sensitive to the mass of the calcium atoms. In fact, Fitzgerald [61] pointed out that the mass for an isotope of calcium provided a better comparison with the data. This observation was substantiated by the bio–mechanics/medical researchers [62].

If the influence of particular atoms appears in such a sensitive manner in vibrating bone, it is to be expected that the sensitive influence of certain atomic elements will be found in shock–loaded materials such as polymers, compounds, and mixtures of compounds.

If Equation C–1 is multiplied by h, it is equivalent to Equation 12.59 in Reference 41, for the energy of a particle in a one dimensional box (or line segment).

DISTRIBUTION LIST

	Copies
AMSMI–RD, ATTN: Peggy Doran/Mr. Walter Jennings	2
AMSMI–RD–CS–R	15
AMSMI–RD–CS–T	5
AMSMI–GC–IP, Mr. Fred H. Bush	1
U.S. Army Materiel System Analysis Activity ATTN: AMXSY–MP (Herbert Cohen) Aberdeen Proving Ground, MD 21005	1
IIT Research Institute ATTN: GACIAC 10 W. 35th Street Chicago, IL 60616	3
Sandia National Laboratories ATTN: Dr. D. D. Bloomquist P. O. Box 5800 Division 1252 Albuquerque, NM 87185	3
Los Alamos National Laboratory ATTN: Dr. Steven A. Sheffield Group M–9 Mail Stop P–952 Los Alamos, NM 87545	3
Terminal Ballistics Division SLCBR–TB, Dr. A. Mark Aberdeen Proving Ground, MD 21005–5066	3
Explosives Effects Branch ATTN: SLCBR–TB–EE, Dr. R. Frey/Dr. V. M. Boyle Aberdeen Proving Ground, MD 21005–5066	3
Los Alamos National Laboratory ATTN: Dr. I. E. Lindstrom Group WX–5 Mail Stop G–780 Box 1663 Los Alamos, NM 87545	3
Dr. Thomas J. Ahrens Division of Geological and Planetary Sciences California Institute of Technology Pasadena, CA 91125	3

	Copies
Baldini Resource Associates, Inc. 10 Barry Lane Newton, NJ 07860	3
Dr. Manfred Held MBB Verteid Igungssysteme Postfach 1340 8898 Schroben Hausen, Germany	3
ATTN: Dr. Ted Nicholas WRDC–M' LN Wright–Patterson AFB, OH 45433	3
Naval Surface Weapons Center ATTN: R12, Dr. J. M. Short White Oak Silver Spring, MD 20903–5000	3
Naval Surface Warfare Center ATTN: Mr. Tom Wasmund Code G–13 Dahlgren, VA 22448	3
Eglin Air Force Base ATTN: 3246 Test Wing/TZLV, Mr. Bill Dyess Eglin AFB, FL 32542–5000	3
Mr. J. W. Watt 4068 Adams Drive Silver Spring, MD 20902	3
Eglin Air Force Base ATTN: AD/ALJW, Dr. Joe Foster Eglin AFB, FL 32542–5000	3
TASC ATTN: Mr. Charles E. Clucus 907 Mar–Walt Drive Fort Walton Beach, FL 32548	2
UAH Research Institute ATTN: Mr. C. L. Adams Dr. B. Z. Jenkins Huntsville, AL 35816	 5 1

	Copies
Johns Hopkins University ATTN: Professor E. R. Fitzgerald 127 Latrobe Hall 34th and Charles Street Baltimore, MD 21218	10
University of Illinois Department of Aeronautical Engineering ATTN: Professor R. A. Strehlow Urbana, IL 61801	3
One Daniel Burnham Court ATTN: Dr. S. W. Yuan Apartment 1222 San Francisco, CA 94109	2
Los Alamos National Laboratory Dr. James P. Ritchie, Group Leader, Detonation Theory and Applications P. O. Box 1663 M. S. B214 Los Alamos, NM 87545	3
Sandia National Laboratories Dr. Mark B. Boslough, Member Technical Staff Shock Wave and Explosion Physics P. O. Box 5800, Div. 1153 Albuquerque, NM 87185	3
Ms. Brigitta Dobratz 543 Todd Loop Los Alamos, NM 87544	2
Dr. W. C. Davis, President Energetic Dynamics 693 4th Street Los Alamos, NM 87544	2
Mr. James Dahm Safety Consulting Engineers, Inc. 5240 Pearl Street Rosemont, IL 60018	2
Sandia National Laboratory ATTN: Dr. G. I. Kerley P. O. Box 5800 Division 1533 Albuquerque, NM 87185	3

	Copies
Lawrence Livermore National Laboratory ATTN: Dr. M. Van Thiel P. O. Box 808, L–299 Livermore, CA 94550	3
Lawrence Livermore National Laboratory ATTN: Dr. Richard J. Wasley P. O. Box 808 Livermore, CA 94550	3
Commander, U. S. ARDEC SMCAR–AEE–W(W) ATTN: Mr. B. Fishburn Picatinny Arsenal, NJ 07806–5000	3
Commander, U. S. ARDEC SMCAR–CCH–V ATTN: Mr. Floyd Hildebrant Picatinny Arsenal, NJ 07806–5000	3
Dr. Michael R. Edwards Royal Military College of Science Department of Mechanical and Civil Engineering Shrivenham, Swindon, Wilts SN68LA, United Kingdom	1
Office of Weapons Safety ATTN: Dr. Charles Karnes Science Advisor D. P. 22 U. S. Department of Energy Washington, D. C. 20545	3
Sandia National Laboratory ATTN: R. A. Graham P. O. Box 5800 ORG, 1153 Albuquerque, NM 87185	3
Denver Research Institute University of Denver ATTN: Mr. Larry Brown Denver, CO 80208	3
Director, U. S. Army Ballistic Research Laboratory ATTN: Dr. John H. Suckling SLCBR–VL–V Aberdeen Proving Ground, MD 21005–5066	3

	Copies
Director, U. S. Army Ballistic Research Laboratory ATTN: Dr. T. N. Wright SLCBR–TB Aberdeen Proving Ground, MD 21005–5066	3
Argonne National Laboratory Technical Information Services Report Unit BLDG. 203 Argonne, IL 60439	3
Department of Mechanical and Aerospace Engineering ATTN: Dr. Yukie Horie North Carolina State University Raleigh, NC 27695	2
Department of Mathematics ATTN: Dr. Julian Wu North Carolina State University Raleigh, NC 27695	2
Director, U. S. Army Research Office SLCRO–MS, Dr. Kailasam Iyer Dr. Michel Cistan P. O. Box 12211 Research Triangle Park, NC 27709–2211	2
Los Alamos National Laboratory ATTN: Dr. J. J. Dick M–9 Mail Stop P952 Los Alamos, NM 87545	3
Los Alamos National Laboratory ATTN: Dr. Jerry Wackerle P. O. Box 1663 Mail Stop P952 Los Alamos, NM 87545	3
Department of Physics ATTN: Dr. G. E. Duvall Washington State University Pullman, WA 99164–2814	3
Dr. Y. M. Gupta Shock Dynamics Laboratory Department of Physics Washington State University Pullman, WA 99164–2814	3

	Copies
Mr. H. C. Rodean Lawrence Livermore Natinal Laboratory Mail Code 262 P. O. Box 808 Livermore, CA 94550	3
University of Texas at Austin Dept. of Aerospace Engineering and Engineering Mechanics ATTN: Dr. J. C. Westkaemper Dr. C. H. Yew Dr. E. A. Ripperger W. R. Woolrich Labs Austin, TX 78712–1085	3
Mr. Henry W. Bach SMCCR–MUC Chemical Research, Development, and Engineering Center Aberdeen Proving Ground, MD 21010–5423	3
Dr. M. M. Chaudhri/Dr. J. E. Field Cavendish Laboratory University of Cambridge Madingley Road Cambridge CB30HE England	3
Dr. Henry Eyring Department of Chemistry University of Utah Salt Lake City, UT	3
Dr. Franklin Walker Interplay 18 Shadow Lake Road Danville, CA 94526	2
Dr. James Thoreen Air Force Arament Laboratory AFATL/MN Eglin AFB, FL 32542–5000	3
Dr. Allen J. Tullis IIT Research Institute 10 W. 35th Street Cnicage, IL 60616	2
Mr. B. G. Craig 56 Hidden Cove Valparaiso, FL 32580	2

	Copies
Dr. Phillip M. Howe Los Alamos National Laboratory P. O. Box 1663 ATAC, K574 Los Alamos, NM 87545	3
Dr. Michael Cowperswaite SRI International 333 Ravenswood Menlo Park, CA 94025	3
Kaman Sciences Corp. ATTN: Dr. James Wilbeck/Mr. T. S. Pendergrass P. O. Box 2486 Huntsville, AL 35804–2486	3
Dr. Julius Roth Consultant 308 Canyon Drive Portola Valley, CA 94025	2
Dr. Ruth Doherty Naval Surface Warfare Center Bldg. 30, Rm. 110 Silver Springs, MD 20904	3
Dr. B. D. Lambourn Atomic Weapons Establishment Aldermaston (AWE) Reading, RG74PR England	3
Dr. Pers – Anders Persson Center for Explosive Technology Research Campus Station Socorro, NM 87801	3
Dr. Claude Fauquignon Institute Saint–Louis (ISL) 12, Rue De I'Industrie Saint Lous 68301, France	3
Naval Research Laboratory Dynamics of Solids Branch Condensed Material and Radiation Sciences Division ATTN: Andrew E. Williams Washington, D. C. 20375–5000	3
Rudolph L. Zadnik Potomac Research, Inc. Alexandria, VA 22312–2707	3

Commander 3
U. S. Ballistics Research Laboratory
SLCBR–VL–L (ATTN: Mr. Ron Hendry)
Aberdeen Proving Ground, MD 21005

Gencorp Aerojet 3
Dr. Joe Carleone
Mr. Roy Iketani
Mr. Richard West
P. O. Box 296
1100 West Hollyvale Street
Azusa, CA 91702

Dwight J. Jones/W. B. Thomas 3
Thiokol
P. O. Box 400006
Huntsville, AL 35815–1506

Dr. M. H. Rice 2
Systems Science and Software
P. O. Box 1620
La Jolla, CA 92038

Los Alamos National Laboratory 4
ATTN: Dr. J. M. walsh
Dr. R. G. McQueen
Dr. S. P. Marsh
Dr. J. W. Taylor
P. O. Box 1663
Los Alamos, NM 87545

Paul A. Urtiew 1
Lawrence Livermore National Laboratory
P. O. Box 808, L–282
Livermore, CA 94550

Craig M. Tarver 1
Lawrence Livermore National Laboratory
P. O. Box 808, L–282
Livermore, CA 94550

LeRoy G. Green 1
Lawrence Livermore National Laboratory
P. O. Box 808, L–282
Livermore, CA 94550

John W. Kury 1
Lawrence Livermore National Laboratory
P. O. Box 808, L–282
Livermore, CA 94550

	Copies
Edward L. Lee Lawrence Livermore National Laboratory P. O. Box 808, L–282 Livermore, CA 94550	1
Donald L. Omellas Lawrence Livermore National Laboratory P. O. Box 808, L–282 Livermore, CA 94550	1
Arnold Karo Lawrence Livermore National Laboratory P. O. Box 808, L–325 Livermore, CA 94550	1
Walter Herrmann Sandia National Laboratories P. O. Box 5800, Div. 1500 Albuquerque, NM 87185	1
Dennis B. Hayes Sandia National Laboratories P. O. Box 5800, Div. 1530 Albuquerque, NM 87185–5800	1
C. S. Coffey Naval Surface Warfare Center 10901 New Hampshire Ave. Silver Springs, MD 20903–5000	1
Richard Bardo Naval Surface Warfare Center 10901 New Hampshire Ave. Silver Spring, MD 20903–5000	1
Charles Dickinson Naval Surface Warfare Center 10901 New Hampshire Ave. Silver Spring, MD 20903–5000	1
Sigmund J. Jacobs Advanced Technology and Research 1208 Ruppert Road Silver Spring, MD 20903–5000	1
Donna Price Advanced Technology and Research 10901 New Hampshire Ave. Silver Spring, MD 20903–5000	1

	Copies
John Starkenberg U. S. Army Ballistic Research Laboratory Aberdeen Proving Ground, MD 21005–5066	1
Richard C. Harrison U. S. Army Ballistic Research Laboratory SLCBR–TM–EE Aberdeen Proving Ground, MD 21005	1
Douglas E. Kooker U. S. Army Ballistic Research Laboratory Aberdeen Proving Ground, MD 21005–5066	1
Sam Lambrakos Naval Research Laboratory 4555 Overlook Ave., S.W. Washington, DC 20375	1
William E. Deal Los Alamos National Laboratory P. O. Box 1663, MS P915 Los Alamos, NM 87545	1
Charles A. Forest Los Alamos National Laboratory P. O. Box 1663, MS P952 Los Alamos, NM 87545	1
Charles E. Morris Los Alamos National Laboratory P. O. Box 1663, MS J970 Los Alamos, NM 87545	1
Pei Chi Chou Dyna East Corporation 3201 Arch Street Philadelphia, PA 19014	2
Murray Komhauser 3C Systems, Inc. 620 Argyle Rd. Wynnewood, PA 19096	2
Julius W. Enig Enig Associates, Inc. 11120 New Hampshire Ave. Silver Spring, MD 20904	2

	Copies
Graeme A. Leiper ICI Explosives Nobels Explosives Co., Ltd. Stevenson, Ayshire, KA20 3LN UK	2
Hugh R. James Atomic Weapons Establishment Foulness Island, Southend on Sea Essex, SS3 9XE UK	2
Henry H. P. Moulard Institut Saint–Louis (ISL) 12, Rue De I'Industrie Saint Louis 68300 France	2
Algot Persson Swedish Detonic Research Foundation Box 32058, S–12611 Stockholm, Sweden	2
Sandia National Laboratories Thermochemical and Physical Division 1534, ATTN: Dr. J. E. Dunn Dr. D. E. Grady Albequerque, NM 87185	2
Sandia National Laboratories Computational Physics and Mechanical Division 15 31 ATTN: Dr. J. W. Swegle Albequerque, NM 87185	1
Sandia National Laboratory ATTN: Dr. L. M. Barker Albequerque, NM 87185	1
RAFAEL ATTN: Dr. Y. Partom Dr. Z. Rosenberg P. O. Box 2250 Haifa, 31021, Israel	2
A. Garn Butcher Hercules Inc. P. O. Box 98 Magna, UT 84037	2

		Copies
David Mann U. S. Army Research Office P. O. Box 1221 Research Triangle Park, NC 27709		3
AMSMI–RD–W	Dr. Wharton	3
AMSMI–RD–PR	Dr. Stephens/Mr. R. W. Milton	3
AMSMI–RD–WC,	Dr. J. S. Bennett Dr. Miles Holloman	3
AMSMI–RD–SS,	Dr. Grider Mr. Davis	1 1
AMSMI–RD–SS–SE,	Mr. Grabney Mr. Jordan Mr. Waddle	1 1 1
AMSMI–RD–SS–AA,	Dr. Billingsley Mr. Head Dr. Oliver Mr. Ward Ms. Crow Ms. Cornelius	10 1 1 1 1 1
AMSMI–RD–ST–CM,	Mr. Parker Mr. Howard	1 1
AMSMI–RD–ST–WF,	Mr. Schexnayder Ms. Kraft Mr. Lovelace Mr. Lienau Mr. Hill Mr. Cornelius Mr. MacDonald	1 1 1 1 1 1 1
AMSMI–RD–PR,	Dr. O. E. Ayers	1
AMSMI–RD–PR–T,	Mr. L. B. Thorn	1
AMSMI–RD–PR–S,	Dr. J. A. Murfree	1
AMSMI–RD–PR–M,	Mr. Kelly McGuire	1